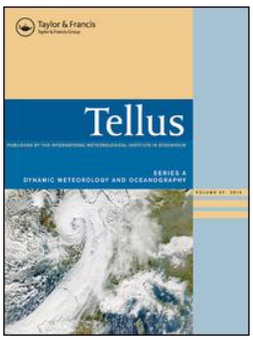

Tellus A: Dynamic Meteorology and Oceanography

ISSN: (Print) 1600-0870 (Online) Journal homepage: http://www.tandfonline.com/loi/zela20

High-resolution ensemble prediction of a polar low development

JØRn Kristiansen, Silje Lund SØRland, Trond Iversen, Dag BjØRge & Morten ØDegaard KØLtzow

To cite this article: JØRn Kristiansen, Silje Lund SØRland, Trond Iversen, Dag BjØRge & Morten ØDegaard KØLtzow (2011) High-resolution ensemble prediction of a polar low development, Tellus A: Dynamic Meteorology and Oceanography, 63:3, 585-604, DOI: 10.1111/j.1600-0870.2010.00498.x

To link to this article: https://doi.org/10.1111/j.1600-0870.2010.00498.x

Tellus SERIES A DYNAMIC METEOROLOGY AND OCEANOGRAPHY
PUBLISHED BY THE INTERNATIONAL METEOROLOGICAL INSTITUTE IN STOCKHOLM

Tellus (2011), 63A, 585–604
Printed in Singapore. All rights reserved

TELLUS

High-resolution ensemble prediction of a polar low development

By JØRN KRISTIANSEN[1]*, SILJE LUND SØRLAND[1], TROND IVERSEN[1,2], DAG BJØRGE[1] and MORTEN ØDEGAARD KØLTZOW[1], [1]*Norwegian Meteorological Institute (met.no), Oslo, Norway;* [2]*Department of Geosciences, University of Oslo, Norway*

(Manuscript received 15 April 2010; in final form 29 November 2010)

ABSTRACT

Severe weather is frequently associated with polar lows over ice-free waters during Arctic winter. We propose a high-resolution, limited area ensemble prediction system (EPS) to enable early warnings of such events. The system (UMEPS) employs the UK Met Office non-hydrostatic Unified Model at 4-km resolution to downscale the 21 ensemble members of the HIRLAM-based LAMEPS run twice daily with 12-km resolution at met.no since February 2008. LAMEPS includes a 3DVar-based control forecast, although initial and boundary perturbations are taken from a version of EPS at ECMWF with perturbations targeted to Northern Europe (TEPS). The added value of UMEPS is evaluated for one polar low during the March 2008 IPY-THORPEX campaign. Forecast probabilities, pseudo-satellite pictures, polar low tracks and strike probability maps are compared with observational data. The forecast quality depends crucially on the size and location of the UMEPS domain. When sufficiently large, the influence from data imposed at the lateral boundaries can be reduced by a careful domain selection. The results are sensitive to the model's parameterizations of physical processes. Although preliminary, this study indicates that with a short-range, high-resolution UMEPS, potentially valuable warnings of extreme weather can be given up to 2 days in advance.

1. Introduction

During the extended winter season the ice-free ocean areas east of Greenland and north of ca. 55–60°N (the Greenland Sea, the Norwegian Sea, the Barents Sea and the North Sea) are prone to polar lows. These are short-lived (1–2 days from initiation to decay), intense meso-scale (100- to 1000-km diameter) weather systems that develop because of processes unique to the Polar Regions (Rabbe, 1975; Rasmussen, 1983; Businger, 1985; Wilhelmsen, 1985; Harold et al., 1999; Rasmussen and Turner, 2003). They occur with irregular intervals several times each winter month (Blechschmidt, 2008; Bracegirdle and Gray, 2008), and are frequently accompanied by severe weather such as intense heavy precipitation and strong winds. Even though their power decays quickly after landfall, polar lows often put human life and property, as well as the natural environment, at great risk both at sea and onshore. They are particularly dangerous due to their small-scale and fast development. The awareness of polar lows has been considerable among weather forecasters and atmospheric scientists over several decades (e.g. Rabbe, 1975; Økland, 1977; Rasmussen, 1979, 1983; Nordeng, 1990; Nordeng and Rasmussen, 1992); see also Polar Low Special Issue (1985) and Rasmussen and Turner (2003) and references therein. Even though there is now considerable understanding of polar lows, and numerical weather prediction (NWP) models, data assimilation methods and remote sensing observations have reached far with respect to resolution and sophistication, the prediction of these and other related extreme Arctic weather phenomena frequently fails. Therefore, polar lows are still intensively studied, for example as part of the International Polar Year (IPY, see http://www.ipy.org/projects/item/263-thorpex-ipy-improved-numerical-weather-forecasting-and-climate-simulations).

Polar lows are often preceded by an outbreak of statically stable Arctic air masses flowing from an ice-covered ocean or a land surface to a much warmer open ocean surface, resulting in strong vertical turbulent fluxes of heat and moisture from the ground surface and a reduced static stability in the lower troposphere. Trigger mechanisms for polar lows are frequently associated with the existence of a mobile potential vorticity (PV) anomaly in the free troposphere, that is a cold upper-level trough, or a low-level baroclinic zone (e.g. Hoskins et al., 1985; Nordeng,

*Corresponding author.
Norwegian Meteorological Institute, Post Box 43 Blindern, N-0313 Oslo, Norway.
e-mail: jorn.kristiansen@met.no
DOI: 10.1111/j.1600-0870.2010.00498.x

1990; Nordeng and Rasmussen, 1992; Noer and Ovhed, 2003). There are several forcing and instability mechanisms responsible for the triggering, development and intensification of polar lows (e.g. Rasmussen, 1979; Bratseth, 1985; Emanuel and Rotunno, 1989; Montgomery and Farrell, 1992; Yanase and Niino, 2007), and one therefore sometimes refers to a polar low spectrum (e.g. Rasmussen and Turner, 2003; Kolstad, 2006) rather than a common phenomenon. Nevertheless, numerical experiments have shown that without large fluxes of sensible and latent heat from the ocean to the atmosphere, neither the shallow baroclinic cyclone type nor the convective 'hurricane-like' polar lows with warm cores attain their observed intensity (e.g. Emanuel and Rotunno, 1989; Albright et al., 1995; Nielsen, 1997; Claud et al., 2004).

There are reasons to believe that in situ atmospheric observations over the Arctic oceans are often too sparse to adequately analyse the atmospheric state for perturbations that may develop into polar lows over the coming 1–2 days (see, e.g. Aspelien et al., 2011). This situation is only partly compensated by remote sensing data from polar orbiting satellites (Pailleux et al., 2008, p. 15). Key limitations for a successful assimilation of soundings over polar regions are cloud detection and surface contributions to the measured signal. For instance, because polar stratospheric clouds are difficult to detect, they can alias the temperature signal. Furthermore, because of the lack of profile-type observations at polar latitudes, regular radiosondes are of exceptional value when estimating the forecast initial conditions (Noer and Ovhed, 2003; Pailleux et al., 2008, p. 15). Given the poor data coverage and because polar lows develop quickly, a considerable portion of them are therefore difficult to forecast even with high-resolution NWP models (Noer and Ovhed, 2003). Furthermore, model uncertainties due to subgrid scale parameterizations contribute to forecast error (Orrell et al., 2001), and for polar low development in particular, the forecast quality depends crucially on the representation of moist convection. For limited area models (LAMs), lateral boundary conditions also influence forecasts (Gustafsson et al., 1998), hence the choice of size and position of the model domain is important.

In this paper we study the probabilistic forecasting of a polar low using a high-resolution ensemble prediction system (EPS) designed for forecasting meso-scale severe weather. Because the forecast error growth depends on the actual weather situation, forecast uncertainty should be quantified along with probabilities of occurrence of weather events. Ensemble prediction utilizes ensembles of deterministic forecasts to estimate these quantities (e.g. Buizza, 2002). The system we employ, UMEPS, is based on the non-hydrostatic Unified Model (UM) from the UK Met Office (Davies et al., 2005) with 4-km grid resolution. The high-resolution ensemble is obtained by a dynamical downscaling of each ensemble member of a coarser-resolution (12 km) limited-area EPS called LAMEPS (Frogner and Iversen, 2002). There are no data assimilation for the initial state for UM at 4 km. We discuss the added value provided by the downscaling, as well as the sensitivity of the forecast to the size and position of the integration domain and the parameterizations in the used UM-versions. The recent paper by Bowler and Mylne (2009) leaves some reasons for optimism concerning dynamical downscaling of larger-scale ensemble members. In focus is the polar low that developed in the Norwegian Sea off the coast of Northern Norway on 3–4 March 2008. This incident was thoroughly observed during the IPY-THORPEX campaign (e.g. Linders and Sætra, 2010, hereafter LS10).

UMEPS constitutes the last of a three-step nested EPS at the Norwegian Meteorological Institute (met.no). The basic initial state perturbations are constructed in the first step by calculating singular vectors that are targeted to maximize the total perturbation energy over Northern Europe and parts of the Nordic Seas at 48 h optimization time. The ensemble members and the control forecast from the 4DVar analysis constitute the Targeted EPS (TEPS; Frogner and Iversen, 2001). TEPS is a 21-member configuration of the operational global EPS of the European Centre for Medium-Range Weather Forecasts (ECMWF) run at spectral resolution T399 (ca. 50 km) up to 72 h lead time. In the second step, the quasi-hydrostatic High Resolution Limited Area Model HIRLAM version 7.1.4 (Undén et al., 2002; see http://hirlam.org/ for documentation) is used with increased horizontal resolution and with TEPS providing lateral boundary data and initial state perturbations (Frogner and Iversen, 2002; Frogner et al., 2006). HIRLAM is set up with a 6-hourly 3DVar data assimilation for the control forecast, which is taken to be the first of the 21 LAMEPS ensemble members. Each of the 20 alternative ensemble members is constructed by taking perturbations at initial time and at the boundaries from the TEPS forecasts. In this study we use the latest set-up (see Aspelien et al., 2011). LAMEPS is configured with a horizontal grid mesh of 12 km and run up to 60 h.

There are several reasons to downscale LAMEPS. Despite the fact that the initial and lateral boundary data will not include the fine-scale features directly, dynamical downscaling has proven to have some success (Roberts, 2000, 2007; Lean et al., 2008; Roberts and Lean, 2008). For instance, Roberts and Lean (2008) showed that for broad areas of rain the scale at which the precipitation from a 1 km model satisfactorily matched radar observations was strongly correlated with the scale at which precipitation from the driving 12 km model satisfactorily matched the observations. For more localized rain, the correlation was smaller but still significant. Increased horizontal resolution should generally improve the forecast skill on the meso-scales (e.g. Buizza and Hollingsworth, 2002; Mass et al., 2002). Moist convective processes are important for polar low intensification (e.g. Bracegirdle and Gray, 2008) and the forecasting of these systems may therefore be sensitive to the model representation of moist convection. Although individual convection cells are not fully resolved with a 4-km horizontal grid mesh width, their organization into systems like polar lows may be better described. The UM 4-km model uses a modified convection scheme to

allow the explicit generation of convection in situations when the showers are resolved. This results in better representation of large storms (Roberts, 2003; Lean et al., 2008). Also, 4 km is important as a first step towards better resolution of convection at 1–2 km grid length (e.g. Lean et al., 2008; Roberts and Lean, 2008). With the increase of computational power, the interest in using high-resolution NWP models in short-range EPS is growing, as, for example demonstrated in the Swiss-Italian 'MAP D-PHASE' program (http://www.map.meteoswiss.ch/map-doc/dphase/dphase_info.htm) and as discussed by Hohenegger and Schär (2007).

Compared to deterministic forecasts, the ensemble approach enables more efficient early warnings of potentially severe weather (e.g. Jung et al., 2005; Branković et al., 2008). A 'seamless' probabilistic system for forecasting potentially severe weather ranging from 12 h to the medium range is envisaged at met.no in which the ECMWF EPS (EC-EPS) may depict synoptic scale patterns favourable to the development of the smaller scale systems and thereby provide very early warnings up to 15 days ahead of weather conditions favourable for, for example polar lows. As the event approaches in time, LAMEPS will produce more detailed probabilistic forecasts up to 2–3 days ahead. Finally if the forecast event is sufficiently severe and/or the probability is considered significant, UMEPS can be run on demand and thereby further improve the ability of monitoring the event and help issuing public warnings of severe weather. This mode of work requires UMEPS to be run on pre-selected optional domains and downscale the LAMEPS forecasts ahead of time, for example the second day only. The main goal of this study is to show a first example of the feasibility of applying UMEPS to a single case of a polar low which has been well observed. In a later study, UMEPS will undergo a more extensive (and expensive) validation experiment.

The main reason for running UMEPS on demand is the cost of using a high-resolution non-hydrostatic model to downscale several ensemble members, which simultaneously covers the entire geographical area of interest. A predefined set of UMEPS integration domains will therefore be set-up. However, the forecast quality is sensitive to both domain location and size (e.g. Leduc and Laprise, 2009). For instance, given that coarser-resolution perturbations are imposed continuously at the lateral boundaries, a too small domain may hamper the development of the small-scale features in the area of interest. On the other hand, a too large domain may introduce a detrimental change in the large-scale flow, provided that the lateral boundary data are well predicted by the coarse resolution, driving model (Xue et al., 2007). As a novel approach, the sensitivity to the location and size of the UMEPS domain with respect to a polar low is investigated in this study.

A wide range of products can be produced from ensemble forecasts. In addition to a consensus forecast (e.g. the ensemble-mean), the ensemble spread and probabilities of selected weather events, we also investigate the possibility of tracking polar lows. The motivation is to more easily identify and compare the polar low(s) of the different ensemble members and to calculate strike probability maps. The tracking method is based on the algorithm of Hodges (1994, 1995, 1999), which has been extensively used in several studies for tracking synoptic systems (e.g. Hoskins and Hodges, 2002, 2005; Froude et al., 2007a,b). The method has been refined to deal with the fact that NWP models develop several small-scale vortices during atmospheric conditions favourable for polar low events.

In Section 2, the UMEPS is presented in more detail. A brief description of the polar low case under investigation is given in Section 3, and the analysis methodologies are presented in Section 4 including the tracking procedure. Results are presented and discussed in Section 5, whereas a summary and conclusions are given in Section 6.

2. The high-resolution ensemble prediction system

There are three steps in the preliminary proposed early warning system, TEPS, LAMEPS and UMEPS. Each step produces a 21-member forecast ensemble, but the horizontal resolution increases with each step. Because TEPS, LAMEPS and the combined 42-member ensemble synthesized to NORLAMEPS, are adequately described and evaluated elsewhere (Aspelien et al., 2011), they are only briefly summarized here.

TEPS has been operational for several years as a designated configuration of the (global) EC-EPS system employing the latest model cycle. At the time of the polar low in this study, the cycle was 32r3. This model upgrade resulted in more active model physics and faster growth of perturbations (Bechtold et al., 2008). Before September 2009, TEPS was run once per day starting at 0000 UTC. Since then, the 72 h $T_L399L62$ forecasts are initialized both at 0000 and 1200 UTC. The operational scheme for stochastic physics is included in TEPS (Buizza et al., 1999). The initial state perturbations are constructed from singular vectors (SVs), which maximize the total energy in a target domain after 48 h (optimization time). The resolution of the tangent-linear and adjoint models used to calculate the SVs is T42L62, and apart from simple diffusion, they are adiabatic (Buizza and Palmer, 1995; Molteni et al., 1996). The target domain for the SVs covers parts of Northern Europe and the adjacent Nordic Seas, and is defined by segments of meridians and latitude circles through (82°N, 15°W) at the northwest corner and (50°N, 40°E) at the southeast corner.

TEPS obtains similar patterns of spread as the operational EC-EPS over the first 2 days in the target domain with considerably fewer ensemble members (Frogner and Iversen, 2001). Another way to obtain the same total amount of spread with a subset of the operational Northern Hemisphere EPS members is by simply increasing the initial amplitudes of the perturbations. However, such a 'brute force' method would then inflate the spread elsewhere to compensate for the

degenerated spatial pattern of the perturbations in our domain of interest.

As described in Aspelien et al. (2011), the present LAMEPS uses HIRLAM version 7.1.4 (see documentation at hirlam.org) with a horizontal grid mesh width of 12 km and 60 levels in the vertical below 10 hPa. The model is quasi-hydrostatic and is used by several operational centres in Europe (Undén et al., 2002). The integration domain covers Northern Europe and adjacent sea areas extended to include the Barents Sea. The LAMEPS initial perturbations are the TEPS perturbations valid at forecast length +6 h, but the control run starts from a HIRLAM 3D-Var analysis valid at 0600 or 1800 UTC, respectively, and the forecast length is 60 h. Data imposed at the lateral boundaries are provided from TEPS every 3 h for the 20 ensemble member perturbations and for the control run (Frogner and Iversen, 2002; Frogner et al., 2006). To further account for model uncertainties, alternating LAMEPS members use the Kain-Fritsch/Rasch-Kristjansson (Rasch and Kristjansson, 1998; Kain, 2004; Calvo, 2007; Ivarsson, 2007) or the STRACO (Undén et al., 2002) cloud schemes. The first guess in the data assimilation cycle is taken from a short rerun starting from the previous ECMWF analysis. During the IPY-THORPEX campaign, a number of additional observations were available and assimilated by ECMWF as well as by HIRLAM. Aspelien et al. (2011) show a range of standard probabilistic verification statistics for ca. 2 yr for TEPS, LAMEPS and NORLAMEPS. Very briefly summarized from, for example the continuous rank probability scores (CRPS) the screen temperature and 10 m wind speeds are better forecast with the 21-member LAMEPS than the 51-member EC-EPS for the first couple of days in Northern Europe. For precipitation the difference is highly variable with worse results for LAMEPS in late autumn early winter, slightly better in spring and considerably better in summer when the spatial scale of the precipitation is smaller than in other seasons. MSLP, being dominated by large-scale dynamics, is typically equally good or better with EC-EPS. The combined NORLAMEPS products are more consistently better than EC-EPS, TEPS and LAMEPS.

2.1. UMEPS and the UM model configuration

We have used the UM (Cullen et al., 1997; Davies et al., 2005) 4-km model configuration that has been running operationally at met.no since 2008 nested within the deterministic HIRLAM forecast. Currently UM version 6.1 (UM6.1) with 38 levels is being used and most of the experiments presented here are produced with this configuration. The hybrid Sharpest-Louis stable boundary layer vertical mixing scheme is recommended (McCabe and Brown, 2007), however, at met.no the long-tails scheme (eq. 5 in McCabe and Brown, 2007) is employed to enhance the vertical mixing and thereby increase the screen temperatures in stable conditions. Here we present alternative results with the two schemes. Unless stated otherwise, however, the UMEPS results presented below are from UM version 6.1 with Sharpest-Louis mixing in stable boundary layers.

More recently, version 7.3 (UM7.3) has become part of met.no's experimental suite and is also included in this paper for sensitivity studies. The most significant difference between versions 6.1 and 7.3 is the increase in vertical resolution from 38 to 70 levels. In the boundary layer, the number of levels is increased from 13 to 30. The model lid is at 40 km for both vertical resolutions. Other major changes between the two versions are found in the data assimilation system (not employed here), in the parameterization of microphysics and in the coupling between radiation and convection. In UM7.3 it is recommended to reduce the vertical mixing over sea even further by employing the Sharpest scheme (King et al., 2001) over sea but keep Sharpest-Louis over land. However, we found only a marginal sensitivity between Sharpest and Sharpest-Louis over sea, and we will only present results from the former (Sharpest).

Each LAMEPS ensemble member is dynamically downscaled to 4 km by nesting the non-hydrostatic UM within HIRLAM. Hence, LAMEPS provides both initial and hourly lateral boundary conditions to UMEPS. The interpolation from HIRLAM to UM is performed as follows. First, the surface pressure, horizontal wind components, temperature, humidity and cloud liquid water and ice content are bi-cubically interpolated as scalars onto UM's horizontal grid. Then the components of the local wind vectors are redefined according to the rotational direction of the UM grid relative to the HIRLAM grid. Next the horizontally interpolated fields are adjusted to the UM orography preserving the stability structure of the boundary layer. Cubic interpolation in the vertical is then applied to the wind components, humidity, cloud water, cloud ice and temperature (above the HIRLAM lid the UM fields are set constant with height). Finally, the exner function and potential temperature are calculated at the UM levels. Interpolation is also applied to the surface and soil fields. The HIRLAM analysis of sea surface temperature, snow water equivalent and soil temperatures are bi-cubically interpolated in the horizontal, whereas for sea-ice bilinear interpolation is used. The soil temperatures are then redistributed vertically by a simple linear interpolation taking into account the differences in soil layer depths between HIRLAM and UM. Soil moisture content is interpolated from the UK Met Office global analysis. There is no need for vertical interpolation of soil moisture because UMEPS employs the same soil levels as UM global.

2.2. Alternative UMEPS model domains

In this study we have set up three different UMEPS domains which are sketched in Fig. 1. UMEPS-small is square with 300 × 300 grid points, whereas UMEPS-big and UMEPS-bigII both have 390 × 490 grid points. The domain sizes are selected to limit the computational cost and the wall clock

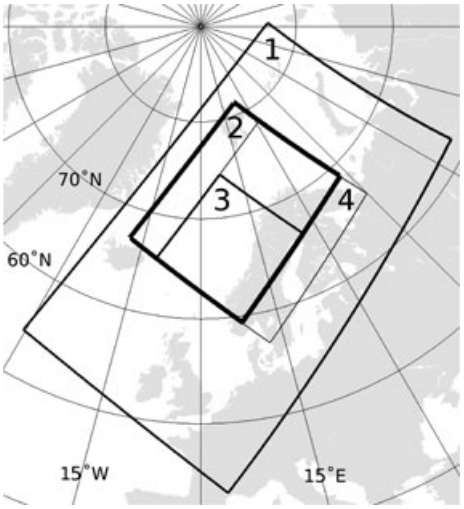

Fig. 1. The model integration domains employed in this study: (1) LAMEPS, (2) UMEPS-big, UMEPS-big* and UMEPS-big7.3, (3) UMEPS-small and UMEPS-small* and (4) UMEPS-big7.3II. See text for details on the different EPS configurations.

run time. The domains all have the same orientation as the LAMEPS grid, all being rotated lat-lon grids with the spherical pole over Greenland (68°N, 320°E). UMEPS-small and UMEPS-big (UMEPS-bigII) have common southeast (southwest) grid corners. The location of the domains was determined subjectively considering the development of the polar low (Section 3) and the proximity to the western lateral boundary of LAMEPS. Given their sizes, UMEPS-big and UMEPS-small are optimally located with respect to the development of the polar low. UM6.1 is employed on domains UMEPS-small and UMEPS-big, whereas UM7.3 is used as an alternative on UMEPS-big (hereafter referred to as UMEPS-big7.3) and UMEPS-bigII (hereafter UMEPS-big7.3II). When UM6.1 is run with long-tails instead of Sharpest-Louis mixing scheme, the systems are referred to as UMEPS-big* and UMEPS-small*. In this way we are able to investigate the sensitivity of the UMEPS results to the size of the domain, the position of the domain and to the choice of model version.

In this study, each of the different UMEPS configurations downscale the LAMEPS forecast initialized at 1800 UTC 2 March 2008. All forecasts are 60-h long. The TEPS forecast providing boundary data to LAMEPS was initialized at 1200 UTC the same day, that is it is 6 h older due to the late operational production time at ECMWF.

3. The 3–4 March 2008 polar low event

In this study, we investigate the performance of UMEPS with respect to forecasting a polar low that developed 3–4 March 2008. The cyclogenesis, the early development and the mature stage of the polar low were extensively observed during an aircraft campaign organized by the Norwegian IPY-THORPEX project (LS10). From the campaign headquarters at Andøya in Northern Norway (69°N, 16°E), the aircraft conducted three flights releasing a total of 54 dropsondes during the life-cycle of the low (Table 1 and Fig. 2). Very few, if any, polar lows have been observed to this extent.

Table 1. Time and duration of the observation flights of the 3–4 March polar low

Flight 1	1000–1400 UTC 3 March 2008
Flight 2	1500–1830 UTC 3 March
Flight 3	1000–1330 UTC 4 March

See text for details.

The reader is referred to LS10 for a comprehensive description of the polar low. Figure 2a shows the infrared (IR) satellite image valid at 1137 UTC together with the HIRLAM 1200 UTC 12 km analysis on 3 March. The 'quicklook' Advanced Very High Resolution Radiometer (ADVHRR) images from the thermal IR channel 4 onboard the National Oceanic and Atmospheric Administration (NOAA) polar orbiting satellites were obtained from the NERC Satellite Receiving Station at the Dundee University in Scotland, UK (http://www.sat.dundee.ac.uk/). A synoptic-scale low was located at about 25°E mid-way between Norway and Svalbard. An Arctic boundary layer front was situated west of Svalbard along the 0° meridian south to about 75°N from where it extended eastward to about 20°E. The front separated the shallow southward flow of cold air masses off the Arctic ice-pack, from warmer maritime air masses advected by easterly winds (see also Fig. 5 in LS10). The surface winds are strong on both sides of the front and the wind speed of the northerly low-level (940 hPa) jet reaches 26 m s^{-1} (Fig. 4 in LS10). Note the front along 70°N separating the Arctic and Polar air masses.

The eye-like cloud structure seen in the IR image at 1721 UTC indicates a small-scale vortex on the Arctic front (Fig. 2b). Small-scale vortices are often seen when there is strong, low-level horizontal wind shear across a narrow Arctic front (Rasmussen and Turner, 2003). Also, the cold air is in its initial stage of wrapping into the warmer air. Flight 2 went over the eye of the low (Fig. 2b), and LS10 propose that the observed relatively warm air with low static stability down to about 800 hPa may be related to intrusion of stratospheric air.

The synoptic-scale, equivalent-barotropic low probably provided sufficient upper-level potential vorticity, which, by interaction with the relatively warm low-level air over the open ocean, caused the vortex to intensify and develop into a polar low (not shown). Around midnight 4 March, the vortex emerged as a meso-scale system on the western flank of the synoptic low (not shown). The polar low further intensified as it followed the large-scale flow towards the Norwegian coast. The IR image

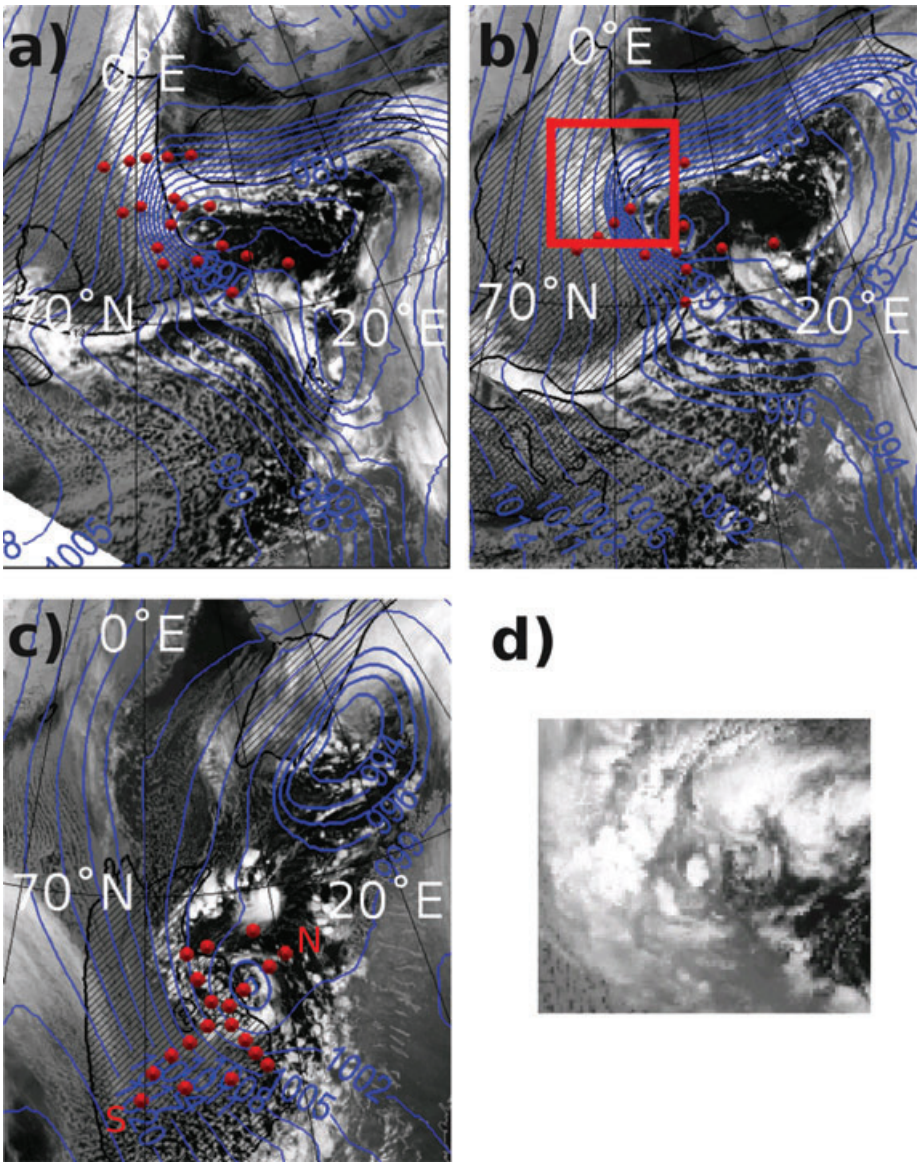

Fig. 2. NOAA IR satellite images channel 4 from (a) 1137 UTC 3 March 2008, (b) 1721 UTC and (c) 1128 UTC 4 March. (d) Enlarged image of the polar low cyclogenesis marked with a red square in (b). The HIRLAM 12 km MSLP analyses are shown as solid blue contours and are valid at (a) 1200, (b) 1800 UTC 3 March and (c) 1200 UTC 4 March. The contour interval is 3 hPa above 996 hPa and 1 hPa below. Following Rasmussen and Turner's (2003) definition of a polar low, the shaded areas show where the wind speeds exceed 13.9 m s^{-1}. Red dots show the positions of the dropsondes released during the three flights spanning the life-cycle of the polar low (Table 1). The section N–S in (c) corresponds to the first leg of Flight 3. In all images, the ice edge is seen in light grey to the west and north of the frontal cloud band.

at 1127 UTC 4 March (Fig. 2c) shows an organized system of convective clouds spiralling around the low centre. The northward stretching tail is the remnant of the convergence zone. The diameter of the low is approximately 500 km and the HIRLAM analysis estimates the central pressure to 996 hPa (Fig. 2c). The dropsondes from the flight leg across the centre of the polar low (marked N–S in Fig. 2c) show a warm core cyclone with low stability up to about mid-troposphere and surrounding convective towers (Figs 7 and 8 in LS10). Again, the observations made in the upper-level air are consistent with stratospheric intrusion, which provides a possible mechanism for maintaining the intensity of the polar low (LS10). The synoptic-scale low is located at about 74°N and 20°E. The polar low made landfall in mid-Norway around 18 UTC on 4 March and the strongest winds (20 m s^{-1}) were observed on the coast of Trøndelag (∼63°N).

4. Analysis methodology

4.1. Ensemble mean, standard deviation, forecast skill and event probabilities

Taking the ensemble mean of the state variables tend to selectively preserve predictable elements in the forecast. It is therefore a valuable supplement to the deterministic forecast (e.g. Zsoter et al., 2009). The unweighted ensemble mean is given by

$$\bar{x} = \frac{1}{n}\sum_{i=1}^{n} x_i, \tag{1}$$

where n is the number of ensemble members (including the control) and x_i is the grid point value of the variable x for ensemble member no. i. In a well-calibrated EPS, the spread between the members gives an indication of the predictability of the actual weather and the expected skill of the ensemble mean forecast. A small ensemble spread should be indicative of high skill of the ensemble mean. A large ensemble spread would normally result in a smooth ensemble mean, indicative of a wide spectrum of unpredictable scales. However, the control forecast (or any single ensemble members) may still be skilful by chance. The ensemble standard deviation measures the ensemble spread or forecast uncertainty:

$$\sigma = \sqrt{\frac{1}{n}\sum_{i=1}^{n}(x_i - \bar{x})^2}. \tag{2}$$

If the ensemble is well calibrated over many cases, the spread about the ensemble mean forecast should measure the skill (root mean square error) of the ensemble mean forecast. Another measure of a good calibration is that predicted probabilities of events are reliable, that is there is agreement between the predicted probabilities and the conditional frequencies of observed events. However, here we only study one single case as an example. For LAMEPS, we use the associated HIRLAM 12-km analysis for verification. However, to calculate the error and skill of the UMEPS ensemble mean, we need to estimate a verifying analysis in the 4-km UM grid. This is done by interpolation of the same 12-km HIRLAM analysis to the respective 4-km UMEPS domains. The scores are largely similar if we instead filter the UMEPS forecast fields to remove the smaller scales and verify against the HIRLAM 12-km analysis.

Ensemble forecasts are frequently used to predict probabilities for the occurrence of selected weather events (e.g. variable $\times$ exceeding a predefined threshold). With a single case study it is clearly not possible to do a full verification of the predicted probabilities. Furthermore, extreme weather events, such as strong winds and intense precipitation associated with polar lows, are rare in nature and therefore difficult to verify. Nevertheless, probabilistic forecasting is particularly important for extreme weather events because even a low probability of a potentially destructive event may provide an important early warning (e.g. Jung et al., 2005).

4.2. Pseudo satellite images

Polar lows can be detected in conventional satellite images, and such images are therefore important for identifying polar lows in otherwise data-sparse areas (Wilhelmsen, 1985; Blechschmidt, 2008). Satellite imagery may also provide an intuitive understanding of the 3-D structure of the weather systems. Hence, we have constructed model-simulated satellite images from the model fields, that is so-called pseudo satellite images. These pseudo images are calculated by using an algorithm originally developed by Tijm (2004) and further developed by Sørland (2009). The IR pseudo satellite images are analogous to conventional satellite IR images derived from terrestrial radiation emitted in the 10–12 μm wavelength band. Pressure, temperature, clouds and ice water content at model levels are used to estimate the IR radiation temperature of the atmospheric column. For grid boxes with thick clouds, the model cloud top temperatures are estimated, whereas for clear skies the surface temperatures are retained. The adapted algorithm and resulting UM pseudo satellite images have been evaluated and validated against the associated IR satellite images for several cases (Sørland, 2009). Largely within forecast uncertainty, the pseudo images are able to reproduce the features seen in the satellite images.

4.3. Tracking polar lows

Several studies have applied a tracking algorithm (e.g. Hodges, 1994, 1995, 1999) to identify synoptic-scale systems and to provide statistical information about their positions, intensities and the genesis and decay (e.g. Hoskins and Hodges, 2002, 2005; Froude et al., 2007a,b). The term track refers to the trajectory of an individual storm, not the average path of many storms. In this study the tracking algorithm is further developed and we investigate the possibilities to track polar lows. Previous studies on synoptic-scale lows have used MSLP or the relative vorticity at 850 hPa (vor850) to identify and track the systems (e.g. Hoskins and Hodges, 2002, 2005; Froude at al., 2007a,b). In addition, we have used the relative vorticity at 925 hPa (vor925). The temporal resolution, or track time step, is 3 h.

First, for each time step the MSLP or vorticity field is decomposed by a discrete cosine transform. A spectral filter then removes the shortest and longest wavelengths. For instance, with a filtering interval of 200–1000 km, features with wavelengths smaller than 200 km and larger than 1000 km are removed, and a new field with positive and negative anomalies is retained. The filtering is employed to select vortices with horizontal scales typical for polar lows. Small-scale features with strong gradients are more easily identified in the vorticity field than in the MSLP field, which is dominated by larger-scale background flow (Hoskins and Hodges, 2002). We therefore use vorticity in the tracking. After the filtering, features associated with sufficiently strong vorticity maxima are tracked by minimizing a cost function (Hodges, 1994, 1995, 1999). The strength of the

Table 2. Summary of the experiments with the tracking algorithm for different combinations of parameter, vorticity threshold and filtering interval

Experiment	Parameter	Vorticity threshold (s^{-1})	Filtering interval (km)	Average number of detected tracks
1	VOR850	2×10^{-5}	200–1000	24
2	VOR850	1×10^{-4}	200–1000	9
3	VOR850	2×10^{-5}	200–600	30
4	VOR850	1×10^{-4}	200–600	6
5	VOR925	2×10^{-5}	200–1000	22
6	VOR925	1×10^{-4}	200–1000	10
7	VOR925	2×10^{-5}	200–600	28
8	VOR925	1×10^{-4}	200–600	8

For each of the eight experiments, the average number of tracks per ensemble member over the entire duration of the ensemble forecast is shown. Each experiment employed the same 21 ensemble members of UMEPS-big and the forecast length was 60 h.

vortices is given by selecting a threshold. Table 2 lists the average number of tracks per ensemble member over the entire duration of the forecast for each combination of filtering interval (200–600 or 200–1000 km), vorticity threshold (2×10^{-5} or 1×10^{-4} s^{-1}) and the level chosen for the vorticity field (vor850 or vor925 hPa). Depending on parameter and filtering interval, the average number of tracks is, two to five times higher with a weaker threshold (2×10^{-5} s^{-1}) than a stronger (1×10^{-4} s^{-1}). For the low-vorticity threshold (2×10^{-5} s^{-1}) the number of tracks increases slightly when the interval is reduced from 200–1000 to 200–600 km. When the vorticity threshold is high (1×10^{-4} s^{-1}) the number decreases when the interval is reduced. The atmospheric processes are generally observed over a broad spectrum of length scales and the filtering may not properly separate the different features (Anderson et al., 2003) unless as shown here, only the stronger vortices are retained.

The tracking is not very sensitive to the choice of the vorticity level (vor850 or vor925). However, the tracks from vor925 tend to identify the systems earlier in the forecasts (not shown). We therefore selected vor925, a vorticity threshold of 1×10^{-4} s^{-1} and a 200–600 km filtering interval. To avoid short lived features, it is required that a vortex must be present over a time period of at least 12 h to be counted as a track. The average number of tracks per ensemble member is then 8, and further objective criteria were introduced to reduce the number further. Analogous to Zahn and Storch (2008) these criteria are: (1) No land requirement: to exclude false disturbances over land the track must start over sea. (2) Strong surface winds: the 10 m wind speed must exceed 13.9 m s^{-1} (moderate gale). (3) Static stability: the temperature differences between the sea surface temperature (SST) and the temperature at 500 hPa must exceed 43 K. In both (2) and (3), the criterion is evaluated within a 1° radius from a given track location and must be fulfilled over at least 20% of the track time steps. In contrasts to Zahn and Storch (2008), these criteria resulted only in a reduction of four to five tracks in total. Interestingly, as in Zahn and Storch (2008), the number of tracks were reduced in LAMEPS (not shown) suggesting a sensitivity to the spatial resolution of the model. Because there are several tracks per ensemble member, we have also selected the track with strongest mean vorticity.

5. Results and discussion

5.1. MSLP forecasts

As mentioned earlier, all forecasts are initialized at 1800 UTC 2 March. The predicted MSLP ensemble mean (eq. 1) and spread (eq. 2) are shown as a function of forecast lead time in Fig. 3 for LAMEPS (left), UMEPS-small (middle) and UMEPS-big (right). The ensemble spread and mean together identify the meteorological features most affected by forecast uncertainty for the actual weather situation. The largest MSLP ensemble spread associated with the polar low is found west of the ensemble mean low, from where the spread extends south-eastward towards the actual position of the real polar low (according to the analysis). This is also where we find the strongest winds (Fig. 2). At the end of the forecast lead time (T + 60), the polar low has made landfall and the associated spread is reduced (not shown).

The ensemble spread is spatially averaged in Fig. 4 and compared to the ensemble mean RMS error as a function of lead time. The averages are taken over the UMEPS-small domain (Fig. 1). The ensemble spread is an estimate of the ensemble mean error and is a priori not expected to match the errors for individual forecasts. Nevertheless, the spread-skill plot is valuable for the comparison of the different ensemble systems and also the feasibility of the UMEPS and LAMEPS during the rare event of a polar low. Apart from the expected result that both the spread and error increase with lead time, there are three noticeable features in Fig. 4. First, as a result of the polar low's proximity to the lateral boundaries, the UMEPS-small forecasts are strongly forced by the LAMEPS forecasts. Hence, UMEPS-small follows LAMEPS quite closely with respect to both spread and error. Secondly, contrary to other ensemble systems (Buizza et al., 2005; Frogner et al., 2006), the forecasts are underdispersive early on in the forecast. The initial lack of spread (spread below 1 hPa) may be a result of employing large-scale SV-based initial state perturbations in the high-resolution ensembles. This is consistent with Jung and Leutbecher (2008), who found that EC-EPS is slightly underdispersive on the subsynoptic scales. The SVs lie along the initial directions, which produce maximum total energy at the optimization time. As such, they are not direct estimates of the actual analysis errors (Buizza and Palmer, 1995; Molteni et al., 1996). Beyond T + 36 (i.e. during the life time of the polar low) the spread in LAMEPS and UMEPS-small matches the ensemble mean error, however, the spread and error are not spatially well correlated. The general

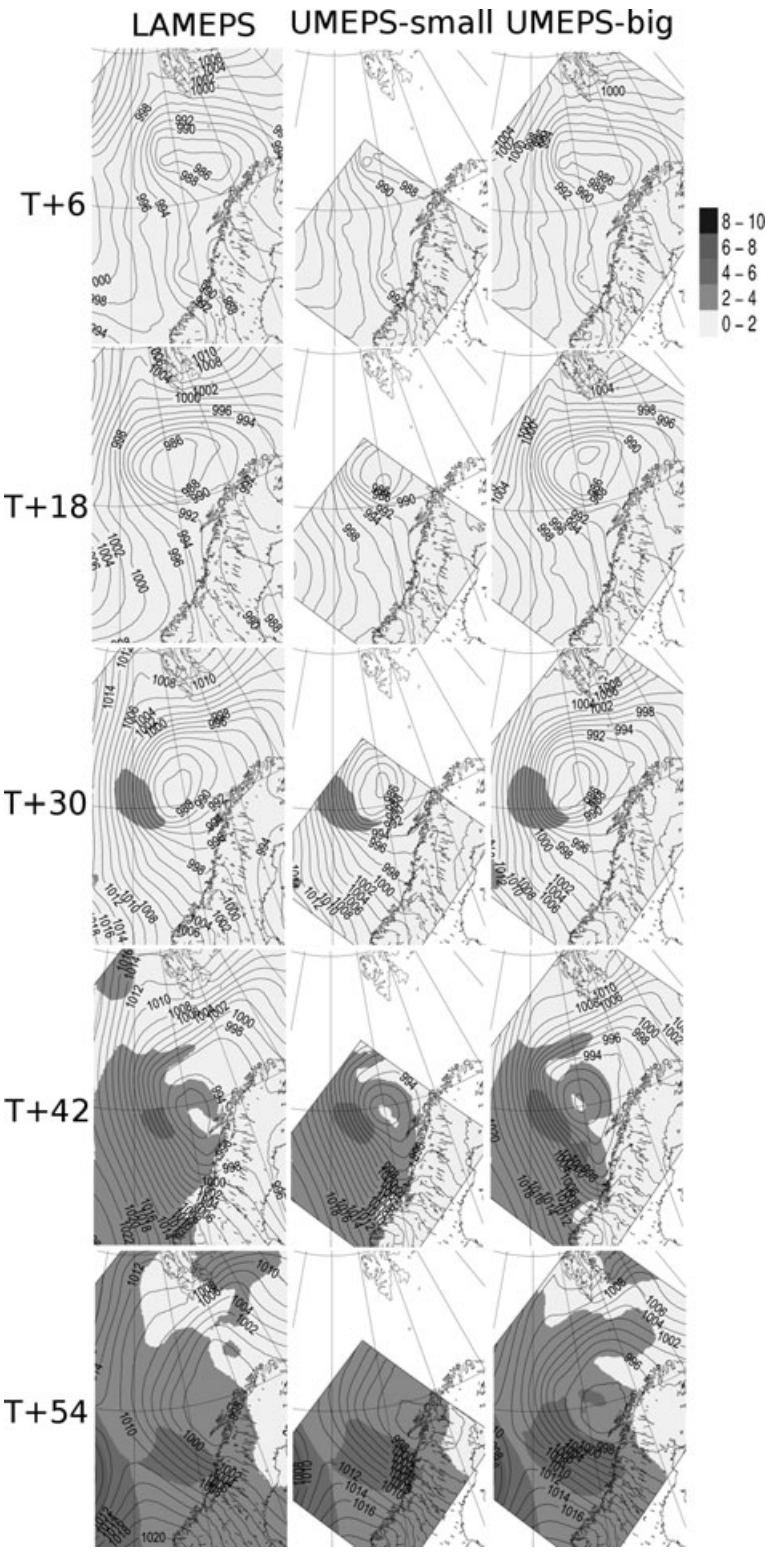

Fig. 3. The MSLP ensemble mean (solid contours) and spread (eq. 2; shaded) from LAMEPS (left column), UMEPS-small (middle column) and UMEPS-big (right column). All forecasts are initialized at 1800 UTC 2 March 2008. Forecast lead times T + 6, T + 18, T + 30, T + 42 and T + 54 are shown. Contour intervals are 3 (1) hPa above (below) 996 hPa for the ensemble mean and 2 hPa for the ensemble spread.

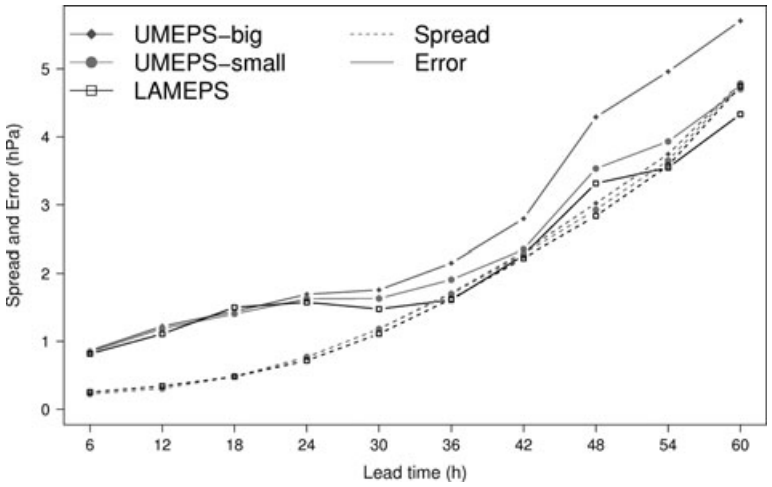

Fig. 4. The average MSLP ensemble mean RMS error (solid) and ensemble spread (eq. 2; dashed) as a function of forecast lead time for LAMEPS (black squares), UMEPS-big (grey diamonds) and UMEPS-small (light grey circles). The scores are spatially averaged over the UMEPS-small domain (Fig. 1) and the verifying analysis is HIRLAM 12 km (i.e. LAMEPS control initial conditions).

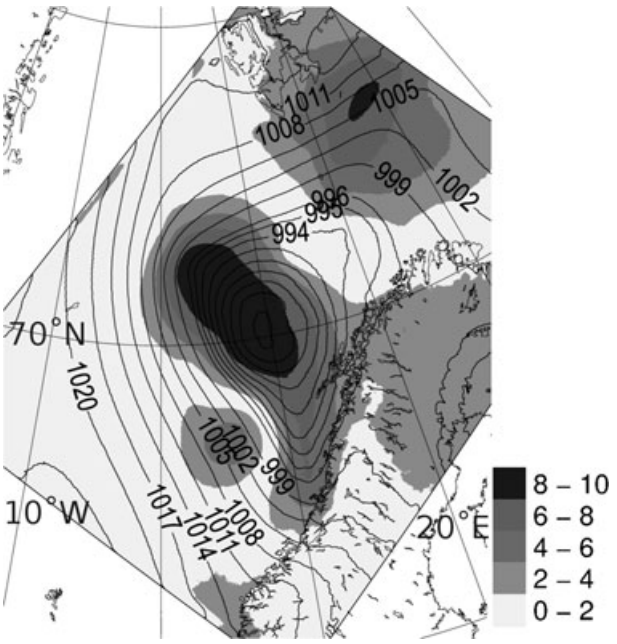

Fig. 5. The MSLP ensemble mean (contours) and error (shaded) for UMEPS-big at T + 42. Contour intervals are 3 (1) hPa above (below) 996 hPa for the ensemble mean and 2 hPa for the ensemble mean error. The ensemble mean error is taken as the difference between the forecast ensemble mean and HIRLAM 12-km analysis.

pattern of the ensemble mean error is similar between the three ensemble systems. The larger ensemble mean error in UMEPS-big (Fig. 5) is mainly a result of the low being deeper and, as seen in the next paragraph, that the synoptic-scale low and the polar low are more spatially separated than in the other two systems. However, this is not reflected in the uncertainty, because the third noticeable feature in Fig. 4 is that the spread is similar in the three ensemble systems (see also Fig. 3).

As seen in Fig. 3, the ensemble means of the three EPS configurations follow different trajectories from about T + 30, that is from when the polar low started to develop. To highlight this difference, the MSLP forecasts of the mature polar low at 12 UTC 4 March (Fig. 2c) are presented in more detail. Fig. 6 shows the MSLP and pseudo satellite images from the T + 42 control forecasts of UMEPS-small (b) and UMEPS-big (c). Unfortunately, pseudo images are not available from LAMEPS (a). By construction, the control forecasts have better initial and lateral boundary conditions than the alternative members. Neither of the control forecasts is able to correctly predict the locations of the polar and synoptic lows. The forecasts position the lows close together with the polar low as a trough to the south of the synoptic-scale low. Hence, the polar low is located too close to the Norwegian coast. The misplacement of the synoptic-scale low affects the large-scale flow and compared to the analysis the forecast wind speed has a stronger easterly component south of Svalbard. The pseudo images indicate little convective activity associated with the forecast polar low, that is contrary to the actual polar low, which was associated with deep moist convection (Fig. 2c).

These results are confirmed by the individual ensemble members and are therefore also reflected in the MSLP ensemble mean and spread (second to last row in Fig. 3) and the individual pseudo images (not shown). For instance, the ensemble spread is small and less than 2 hPa at the centre of the forecast low. However, the polar low is in general more well separated from the synoptic-scale low in the UMEPS-big members and there is a local maximum in the spread where the polar low is located in reality. The trough associated with the small-scaled polar low tends to be smoothed out in the LAMEPS ensemble mean. The difference between UMEPS-big and UMEPS-small ensemble means is largest in the northwest corner of the small domain where the inflow is strong. LAMEPS and UMEPS-small differ only in the depth of the synoptic low. There are also unsystematic differences both between the individual members and between the EPS systems, for example in the number and location of small-scale vortices, the location and areal extent of the strongest wind speeds and the position and strength of the

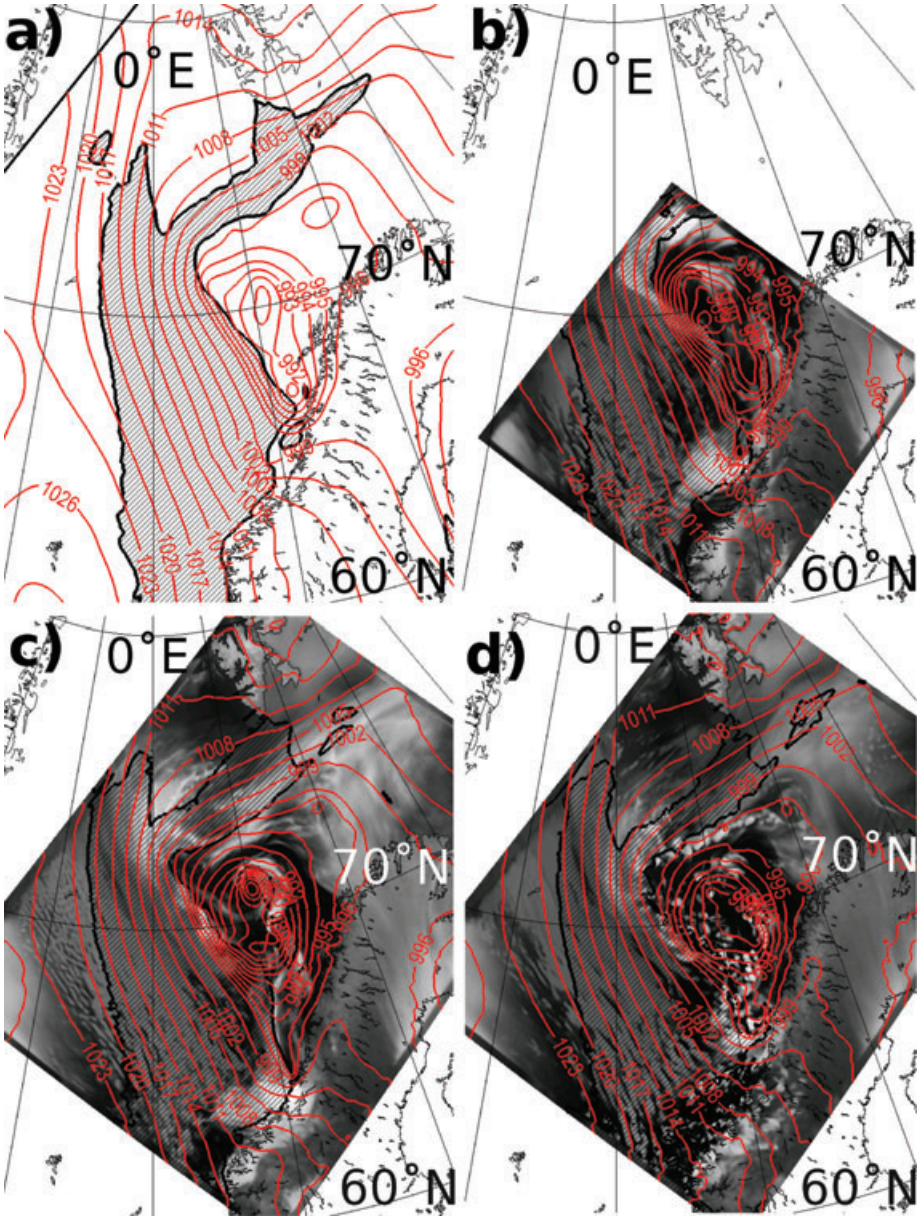

Fig. 6. Same as Fig. 2 but for the ensemble control (unperturbed) forecast of (a) LAMEPS, (b) UMEPS-small, (c) UMEPS-big and (d) UMEPS-big7.3. Note that MSLP is shown as red contours. The pseudo IR images are calculated from the model fields. The forecast lead time is T + 42 corresponding to the observations in Fig. 2c, that is 1200 UTC 4 March. The black shaded areas show where the wind speeds exceed 13.9 m s^{-1}.

deepest vortex (not shown). A more detailed investigation of the forecasts, including a discussion of the processes involved in the development of the polar low, is beyond the scope of this study.

5.2. *Forecast probability of extreme weather*

Figure 7 shows the predicted probability of the event that the horizontal 925 hPa wind speed exceeds 20 and 25 m s^{-1} at lead time T + 42 (1200 UTC 4 March). The associated dropsonde observations are shown as wind arrows. Most wind observations are above 20 m s^{-1} with peak values at 25 m s^{-1}. Both LAMEPS (Fig. 7a) and UMEPS-big (Fig. 7b) estimate that all ensemble members have wind speeds exceeding 20 m s^{-1} over a large spatial region around the observed wind maxima. UMEPS-big has generally higher probabilities than LAMEPS. Qualitatively similar results are found for the other two lead times (T + 18 and T + 24), where we have dropsonde observations (not shown). But the difference between the forecast probabilities of UMEPS-big and LAMEPS is largest at T + 42 when the polar low is at its

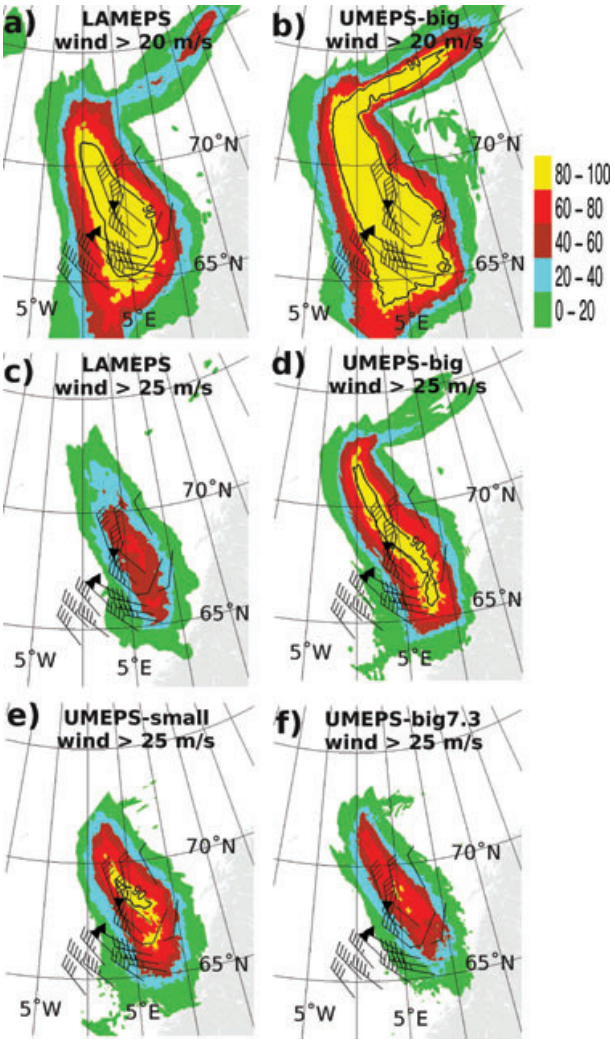

Fig. 7. Probabilities for the occurrence of selected weather events at forecast lead time T + 42 (1200 UTC 4 March 2008). The events are that the horizontal 925 hPa wind speed (a and b) exceeds 20 m s^{-1} and (c–f) 25 m s^{-1}. The contour interval is 20% but in addition the solid line shows the 90% level. The ensemble systems presented are (a,c) LAMEPS, (b,d) UMEPS-big, (e) UMEPS-small and (f) UMEPS-big7.3. The observations are shown as wind arrows where the half barb represents 2.5 m s^{-1}, full barb 5 m s^{-1} and triangle 25 m s^{-1}. The arrows are aligned along the direction of the observed winds.

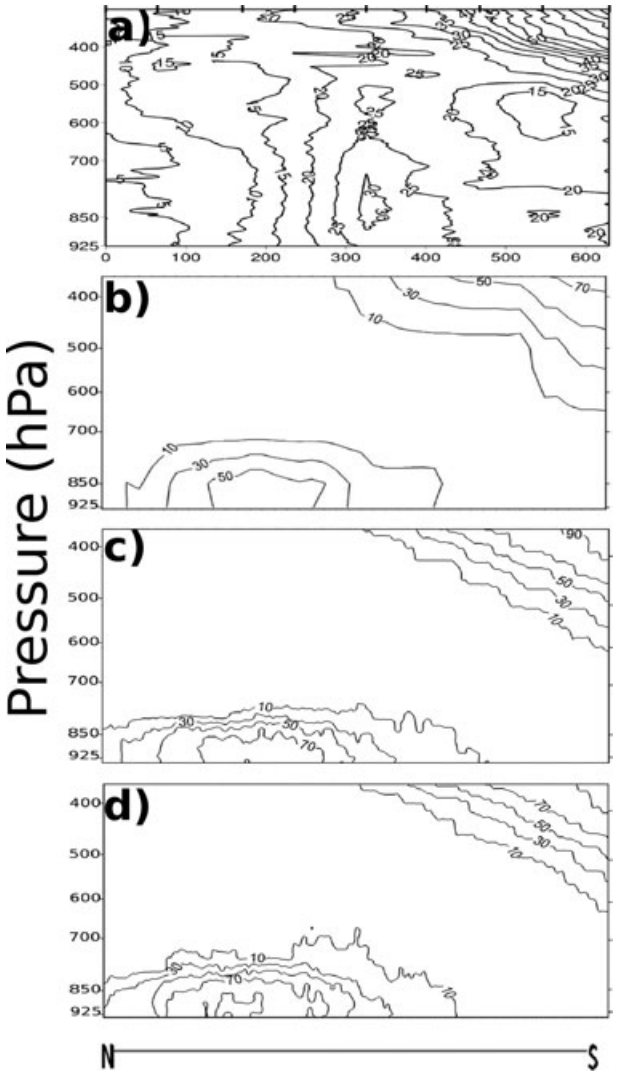

Fig. 8. (a) Vertical cross section of the observed wind speed along the flight leg marked N–S in Fig. 2c. The contour interval is 5 m s^{-1}. The positions of the dropsondes are marked at the top of the panel and the cross section goes from N (left) to S (right). The observations are interpolated spatially. (b–d) Forecast probabilities for the occurrence of wind speeds exceeding 25 m s^{-1} at lead time T + 42 from (b) LAMEPS, (b) UMEPS-small and (c) UMEPS-big along the same cross section as the observations. The contour interval is 20% starting at 10%.

peak. Consistent with the results above, the differences between LAMEPS and UMEPS-small are minor for all lead times (not shown). In agreement with the observations, there are also high probabilities for wind speeds above 25 m s^{-1} (Figs 7c–e). For UMEPS-big (Fig. 7d), the probability is above 90% over a several hundred kilometres long and a few hundred kilometres wide south-eastward orientated band which ends where the real polar low made landfall a few hours later. The probabilities are lower and rarely above 60% in LAMEPS (Fig. 7c). South of Svalbard where UMEPS-big predicts strong winds associated with the remains of the synoptic low, LAMEPS only locally have winds above 25 m s^{-1}. Again, the general pattern of probabilities is similar between UMEPS-small (Fig. 7e) and LAMEPS (Fig. 7c) but the probabilities are generally about 0.25 larger in the former with peak values of 0.9 (i.e. 90%), that is closer to the values in UMEPS-big (Fig. 7d).

Figure 8 shows vertical cross sections of the horizontal wind speed interpolated from the dropsonde observations taken on Flight 3 along the cross section N–S in Fig. 2c and the forecast

probability of wind speeds above 25 m s^{-1}. There are significant non-zero probabilities in the region where the strongest winds are observed. Even though the low-level jet is not forecast with high probability, it is captured within the spread of the ensembles. However, the observations show winds over 25 m s^{-1} at altitudes up to 450 hPa, whereas the forecasts give probabilities of less than 10% above 700 hPa. Again LAMEPS has the lowest and UMEPS-big the highest probabilities. The maximum probabilities in LAMEPS are found close to the height of the observed wind speed maximum at 840 hPa whereas UMEPS place the region of peak probabilities slightly lower and all the way down to the surface. In fact, for the event of wind speeds above 25 m s^{-1} the two UMEPS forecasts are more similar to each other than to LAMEPS. For lower thresholds, UMEPS-small follows LAMPES (not shown). Overall Figs 7 and 8 suggest that forecasting wind speed is sensitive to the model resolution (UM vs. HIRLAM) and the domain size (big vs. small).

Figure 9a shows a composite of precipitation accumulated over 3 h (0900–1200 UTC 4 March) from the ground-based precipitation radars located (from North to South) at Andøya, Røst, Rissa and Bømlo along the Norwegian coast. During this period, the precipitation was located mainly over land covering an extensive region between 62 and 65°N. There are several showers further north along the coast and over the ocean. The clouds associated with the precipitation are visible on the 1128 UTC IR image (Fig. 2c), however, the cloud spirals around the polar low centre are outside the range of the radars. For several small areas the precipitation exceeds 2.5 mm per 3 h, but because the precipitation fell as snow, the amount may have been underestimated by the radars (Lopez, 2008). Forecast probabilities for the event that the precipitation intensity exceeds 2.5 mm per 3 h over the period T + 39 to T + 42 are shown for UMEPS-big in the same panel as the radar observations (a). Most of the observed precipitation is well captured by the ensemble. The region with high probabilities (60–80%) around 65.5°N, 9°E is associated with the polar low. Figures 9b–d compares the forecast probabilities of (b) LAMEPS, (c) UMEPS-small and (d) UMEPS-big for the same event as in (a) but on a larger spatial domain. Figure 9a is thus a subsection of (d), focusing on the region covered by the radars. The spatial distributions of the probabilities are similar between the three EPSs but slightly more so between LAMEPS and UMEPS-small. As for the wind speed, the forecast probabilities are highest in UMEPS-big and lowest in LAMEPS, and the differences are largest over sea. The largest area of high probabilities is co-located with the high forecast probabilities for very strong winds in Fig. 7.

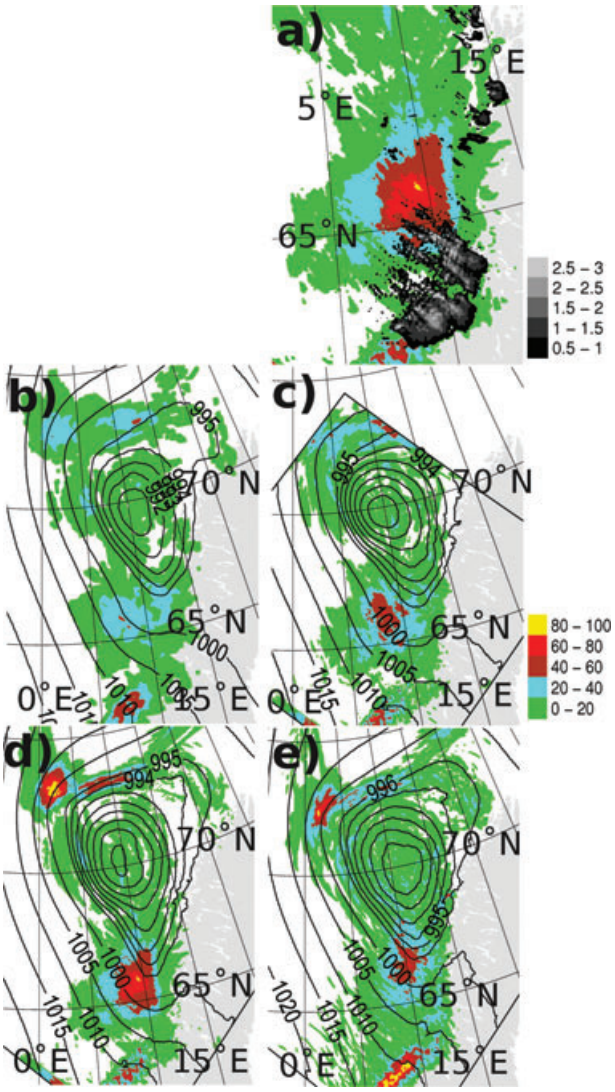

Fig. 9. (a) Grey shading: Composite of observed 3-hourly precipitation accumulations (mm per 3 h) over the period 0900–1200 UTC 4 March 2008. The observations are taken from the ground-based precipitation radars located (from North to South) at Andøya, Røst, Rissa and Bømlo on the Norwegian coast. The contour interval is 0.5 mm per 3 h. Coloured shading: UMEPS-big forecast probabilities for the occurrence of 3h-accumulated precipitation exceeding 2.5 mm per 3 h between lead times T + 39 and T + 42 (0900–1200 UTC 4 March). (b–e) Same as in (a) superposed on the ensemble mean MSLP (solid contours) at T + 42 but for (b) LAMEPS, (c) UMEPS-small, (d) UMEPS-big and (e) UMEPS-big7.3. Note that (a) is a cropped version of (d) but with radar observations superposed. The probabilities are shaded every 20%. The MSLP contour intervals are 5 hPa above and 1 hPa below 996 hPa.

5.3. *Sensitivity to model version, stable boundary layer mixing and domain location*

In this subsection, we illustrate the sensitivity of the results with respect to choices of boundary-layer physics, the UM version and the size and position of the model domains, as described in Section 2.

The different stable boundary layer vertical mixing schemes (Sharpest-Louis and long-tails) have only a minor and

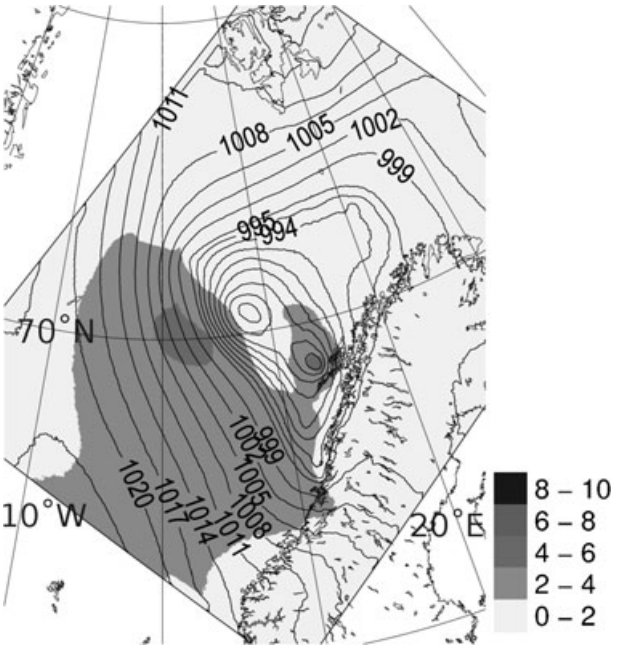

Fig. 10. As Fig. 3 but for UMEPS-big* at lead time T + 42 (1200 UTC 4 March).

insignificant impact on the UMEPS-small forecasts (not shown) but we find a significant impact in UMEPS-big. This is consistent with the previous results that the LAMEPS boundary data strongly influence UMEPS-small, but it could also reflect that the boundary layer is prevailingly unstable within the UMEPS-small domain, see for example Fig. 6. For UMEPS-big, increasing the vertical mixing in the stable boundary layer by employing the long-tails scheme results in two 988 hPa deep lows in the ensemble mean (Fig. 10); one outside Lofoten at about 69°N, 13°E, and the other further to the northwest at about 71°N, 8°E. The latter is located at about the same location as the low found in UMEPS-big with Sharpest-Louis mixing (Figs 6c and 10). However, neither of the two lows is collocated with any of the two lows of the analysis. With the long-tails scheme the forecast probabilities of high wind speeds are generally increased where the observed wind speeds are weak (and vice versa for strong winds; not shown).

The general pattern of MSLP ensemble mean and spread are similar between UMEPS-big7.3 and UMEPS-big but both the synoptic-scale low and the trough associated with the polar low are weaker when UM7.3 is employed (Figs 9d and e). The difference between the probability maps for winds exceeding 20 m s^{-1} is small (not shown). However, the spatial distributions are more spatially confined with version 7.3, and the differences are larger for the higher thresholds, such as for the probabilities of wind speed exceeding 25 m s^{-1} (Fig. 7f) and precipitation amounts exceeding 2.5 mm per 3 h (Fig. 9e). Probably as a consequence of the weaker trough, UMEPS-big7.3 does not forecast as high probabilities as UMEPS-big but is more similar to UMEPS-small. An exception is precipitation over land (Fig. 9e) where UMEPS-big7.3 has higher probabilities.

An interesting feature in version 7.3 compared to 6.1 is the increased spatial detail in the precipitation probabilities with the newer version. Convective showers around the vortex centre are apparently more easily identified in Fig. 9e. This increase in spatial detail is also seen in the pseudo satellite images; as shown in Fig. 6d. Judging from the pseudo images, there is more convective activity in and around the polar low in UM7.3 than in UM6.1, and this is consistent with the IR observations shown in Fig. 2c. Previous studies have noted that the UM 4-km model tends to behave differently depending on whether or not a convective parameterization is included (e.g. Roberts, 2003; Lean et al., 2008). A modified convective parameterization was developed by Roberts (2003) and included in the 4-km model. The scheme allows explicit representation of developing clouds resolved by the model but still represents the effects of weaker convective clouds. Because the most significant difference between UM6.1 and UM7.3 is the number of levels, the increase in deep convective activity between model versions suggests that the modified convective parameterization is sensitive to the vertical grid spacing.

As for the choice of integration domain, UMEPS-big7.3 forecast higher probabilities (about 10%) of the extreme events than UMEPS-big7.3II (not shown). The differences are smaller for lower thresholds and also for the ensemble mean and spread. This suggests that with respect to forecasting the extremes associated with polar lows, UMEPS should employ an integration domain in which the polar lows are able to develop fine scale features without being unduly restricted by the coarser data imposed at the lateral boundaries.

5.4. Polar low path tracks and strike probability maps

Because the polar low was not present in the analysis, it is more difficult to employ the tracking algorithm to determine its spatial path of motion (i.e. its track). In particular, it is not straightforward to define the initial position of those small disturbances that will develop into polar lows. Because polar lows are short-lived systems, it is necessary to be able to identify lows that appear during a forecast as part of an early warning system. Figure 11 shows all tracked paths (left column) and the path of the track with strongest mean vorticity (right column) from all ensemble members as a function of the ensemble configuration. The observed polar low track has been estimated by visual inspection of the IR images and is shown as grey crosses in Fig. 11. From all plots we identify five clusters of paths, which are most easily identified in UMEPS-big7.3 (left column). Cluster 1 is located to the west, Cluster 2 is located close to the trajectory of the observed polar low, Cluster 3 is to the north of Cluster 2 and Cluster 4 is the short arc closest to Svalbard. Cluster 5 is located between and to the east of Clusters 2 and 3. We first consider the composites containing only the strongest track from each

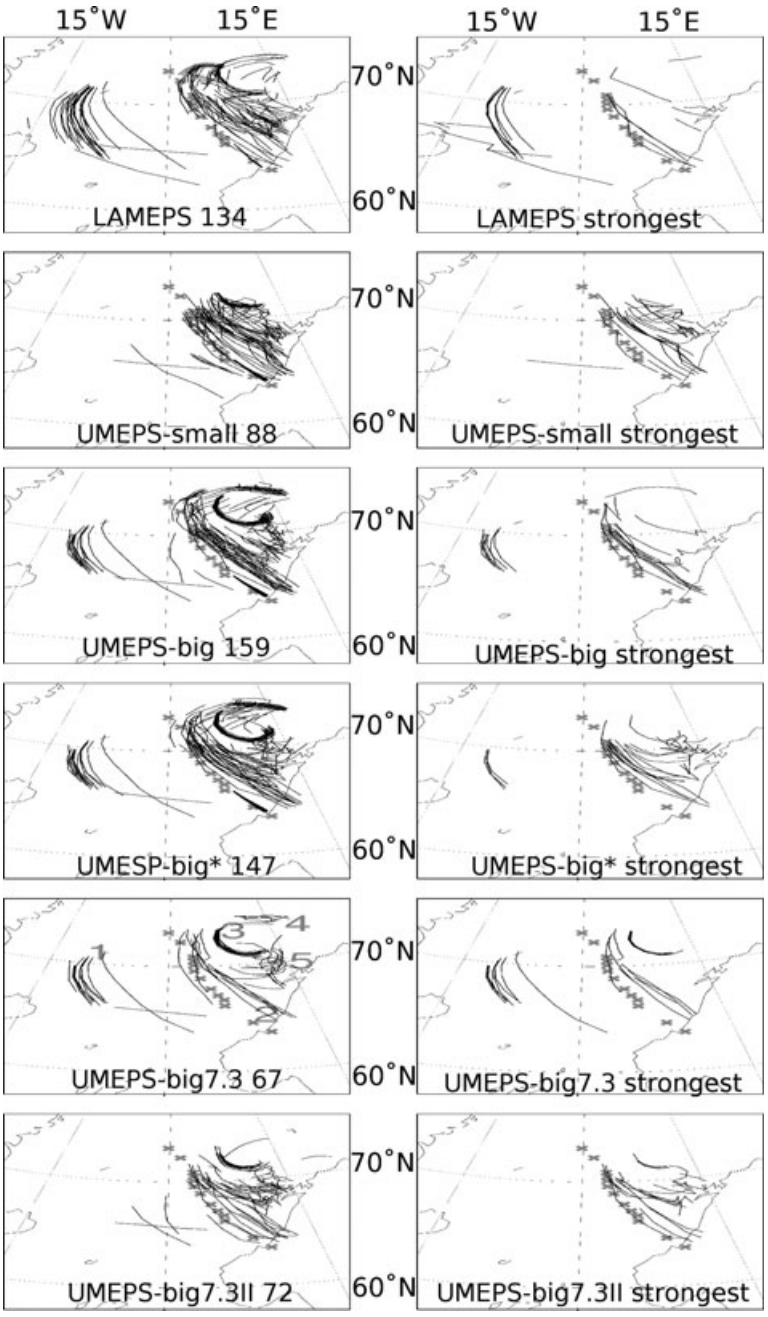

Fig. 11. Polar low tracks. Left panels show all tracks and right panels only the strongest track from each ensemble member. For each EPS configuration, the total numbers of tracked paths are given in the respective panels. See text for details.

ensemble member (right column). Clearly, UMEPS-big is tracked with several paths at almost correct location. However, several tracked paths are also located in Cluster 1. As already noted, the model version 6.1 with increased vertical turbulent mixing in the boundary layer produces a second low in the forecasts, and this is identified as Cluster 5. UMEPS-big7.3 has fewer tracks belonging to Cluster 2, and more to Cluster 1 and Cluster 3, than UMEPS-big. This may explain the lower probabilities of severe weather found in UMEPS-big7.3 as discussed in the previous section, or conversely, the increased probabilities found with increased boundary-layer vertical mixing used in UMEPS-big. UMEPS-small places the tracked paths too far north, and neither in clearly defined clusters. LAMEPS has few path tracks close to the correct location (Cluster 2) and most in connection with Cluster 1, which is located outside the small-sized UMEPS domain.

When we compare the results for *all tracked paths*, the difference is smaller. For each EPS configuration, the total numbers of tracked paths are given in the respective panels of Fig. 11. For the big-sized UMEPS domain, the number of path tracks is

about 150 when UM6.1 is employed. UM7.3 reduces the number of small-scale vortices and thus also the tracks to about 70. LAMEPS has about the same number of tracks as UMEPS-big and at about the same location. In consequence, downscaling is more important for defining the strongest tracks. Except for the strongest tracks, the vertical mixing scheme has little impact on their location. Therefore, the choice of vertical turbulent mixing scheme mainly impacts the strength of the vortices.

Similar to the ECMWF probability forecasts of tropical cyclones (van der Grijn, 2002), strike probability maps for the polar low have been constructed, Fig. 12. The strike probability shows the forecast probability that a polar low will pass within a 48×48 km^2 region from a given location during the next 60 h (the forecast length), that is predicting the location of the centre of the low any time in a 60 h window. The forecast probability is based on the strongest track from each of the EPS members. As for the clusters of tracked paths, the forecast strike probabilities are sensitive to model, domain size and location, and vertical mixing scheme. All EPS configurations forecast that it is likely that the low will follow the actually observed polar low trajectory, but for most of the systems the probability is higher at other locations. These maps strengthen the impression that the best forecast, in terms of the most probable location of the polar low, is obtained with UMEPS-big.

6. Discussion and conclusions

With increased computational power, the high-resolution numerical weather prediction (NWP) models will be able to resolve cloud-scale processes and should thereby improve the forecasts on the meso-scales (e.g. Buizza and Hollingsworth, 2002; Mass et al., 2002). Because prediction uncertainties along with probabilities for rare events are best obtained by using ensemble of forecasts (e.g. Jung et al, 2005; Brankovic et al., 2008), we propose a high-resolution LAM EPS, UMEPS. We discuss various versions of UMEPS with 4-km grid resolution applied to a single case of a polar low, which was extensively observed during a flight campaign during the IPY-THORPEX project. UMEPS dynamically downscales the ensemble members of the HIRLAM-based LAMEPS (Frogner et al., 2006; Aspelien et al., 2011) with

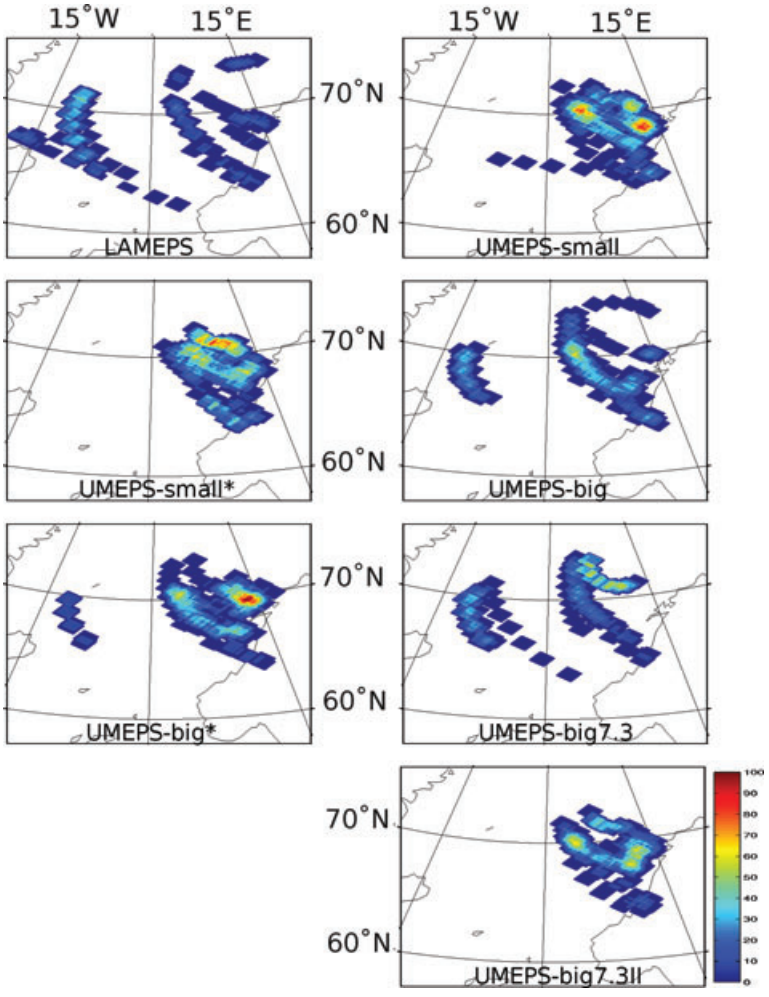

Fig. 12. Polar low strike probability maps. The strike probability predicts the location of the centre of the low any time in a 60 h window. The forecast probability is based on the strongest track from each of the EPS members. See text for details.

the non-hydrostatic UM imported from the UK MetOffice. The initial and lateral boundary conditions of each LAMEPS ensemble member are provided by the targeted version of the ECMWF EPS forecasts (TEPS). Together, it is intended that these three ensemble systems, or their further developed versions, will constitute the basis for improving the Norwegian Meteorological Institute's ability to issue early warnings and monitor the developments of the severe weather associated with polar lows as well as other meso-scale systems. TEPS and LAMEPS have been documented in previous studies (Frogner and Iversen, 2001; Frogner et al., 2006) and the latest version by Aspelien et al. (2011).

This paper present an initial investigation of the potential abilities of UMEPS forecasts, as well as their sensitivities with respect to chosen model domain size, domain location, model version and choice of vertical turbulent mixing scheme in the boundary layer. Extensive observations from the 3–4 March 2008 polar low during the IPY-THORPEX campaign (LS10) have been used to tentatively asses the potential of UMEPS. A cold, equivalent-barotropic synoptic-scale low in the Barents Sea triggered the cold air outbreak which led to the formation of the polar low. It made landfall in mid-Norway on the afternoon the same day. The UMEPS and LAMEPS forecasts were initiated at 1800 UTC 2 March, that is before the polar low started to develop.

Even though we have only investigated one polar low, an ensemble system estimates the forecast uncertainties due to inaccurate initial and lateral boundary condition data. As such, running EPS on one polar low may provide more information on model sensitivity than running deterministic forecasts on several different polar lows. The dynamical structure and the growth mechanisms of polar lows are different, and their end location and relative positions will differ between different cases (see, e.g. Rasmussen and Turner, 2003). That is, our results may be used as first reference in future similar studies. To resolve the convection associated with the polar lows, even finer horizontal grid spacing than 4 km will probably be required (e.g. Yanase and Niino, 2005). Clearly, for still several years to come, such model resolutions will constrain the model domain size considerably.

A novelty of this study is the tracking of polar low paths in a high-resolution (here 4-km grid) model, UMEPS. We identify two challenges. First, there are numerous small-scale vortices in the individual forecast members. Hence, the tracking criteria should be investigated further. Secondly, in an operational setting the aim is to identify the lows as early as possible and the fast developing and short-lived polar lows will frequently not be present in the initial conditions of the UMEPS domain. For the case studied here, the tracking algorithm identified five different clusters of tracked paths, one of which was co-located with the trajectory of the actually observed polar low. The associated strike probabilities differed depending on model, domain size and domain location. UMEPS-big gave a good estimate of the observed polar low trajectory, whereas the other UMEPS configurations had higher probabilities at other locations. The forecast strike probabilities may be particularly useful for forecasters on duty. For instance, they may be used to determine the most likely trajectory and thereby adjust the associated probabilities of associated severe weather such as strong wind and intense precipitation. Polar low path tracks and forecast strike probability maps are also of high potential value for the public user.

The polar low started to develop in the second day of our forecast period. However, the polar low's development and/or interaction with the synoptic-scale low to the east in the Barents Sea were not correctly forecast and both systems were misplaced. Nevertheless, we found that both LAMEPS and UMEPS have the potential to give a warning of extreme weather 1–2 days ahead, and UMEPS forecast the highest probabilities of strong surface wind speeds and intense precipitation. This was especially evident for longer forecast lead times, for the period when the polar low was fully developed. We take these results in support for the basic assumptions behind dynamical downscaling. The value added by the high-resolution UMEPS compared to LAMEPS is sensitive to both model domain size and domain location. With a domain size of 300 $\times$ 300 grid points UMEPS is strongly controlled by the lateral boundary data. A larger domain size (390 $\times$ 490 grid points) permits the UMEPS forecasts to develop more freely on the finer scales, provided the lateral boundaries are sufficiently far from the polar low. We also found that the forecasts appear to be sensitive to model version and choice of stable boundary layer vertical mixing scheme. For instance, compared to model version UM6.1, UM7.3 reduced the number of small-scale vortices in the forecasts and instead increased the convective activity. However, the forecast probabilities are slightly lower, probably because fewer tracks were found close to the actually observed polar low trajectory.

The UMEPS domains (Fig. 1) employed in this study were selected a posteriori. However, in an operational environment where UMEPS is run on demand the model domain needs to be selected a priori. It is planned to prepare up to four domains to be selected from on a given day. Polar lows may develop all over the Nordic and Barents Seas (Bracegirdle and Gray, 2008; Blechschmidt, 2008) and from time to time even over the North Sea (Harold and Browning, 1969; Aakjær, 1992). A typical polar low can be 100–600 km in diameter, lives in a developed phase for 15 h (Blechschmidt, 2008) and moves with a speed of about 10–15 m s^{-1} (36–54 km h^{-1}; Shapiro et al., 1987; Noer and Ovhed, 2003). Consistent with the results in this study, a domain size similar to the UMEPS-big-sized domain (1560 $\times$ 1960 km) may if, favourably placed, be sufficiently large for short-range forecasts of polar lows whereas the UMEPS-small-sized domain (1200 $\times$ 1200 km) will probably be too small. Even with the big-sized domain, a good global or large regional ensemble forecast is needed to guide the choice of domain amongst those that are predefined and prepared. Unfortunately, this is not the case

for all polar lows (e.g. Aspelien et al., 2011). Therefore, an on demand high-resolution forecast system cannot be expected to improve complete failures in the coarser resolution forecasts.

Another weakness of an EPS that is not run regularly is verification. Probabilistic forecasts needs to be produced for a representative number of cases to be verified with standard measures for quality and value. It will be difficult to obtain sufficient data for verification with an on demand system for all the prepared domains.

Moreover, there may not always be an optimal choice of domain even if the pre-defined domains are partly superposed to reduce the proximity to the lateral boundaries. The selection of model domain may therefore introduce uncertainty in the UMEPS forecasts, for example as seen in the comparison between UMEPS-big7.3 and UMEPS-big7.3II. The uncertainty could be reduced by shorter length forecasts (24–36 h) run twice daily where the UMEPS initial time is selected from the LAMEPS forecast lead times, for example T + 0 in UMEPS could correspond to T + 24 in LAMEPS. Given the 60 h forecast length of LAMEPS each polar low would then be sampled by up to four subsequent forecasts.

There is on average 1–1.5 polar lows per week during winter (Blechschmidt, 2008; Bracegirdle and Gray, 2008), and on days without new polar lows the allocated computer resources could be used to run UMEPS on alternative domains. The suggested approach to run UMEPS within an operational environment should give us an estimate of the uncertainty introduced by the choice of model domain as well as provide valuable experience with a high-resolution EPS designed for extreme weather events.

The results presented in this paper are preliminary, and they give confidence to continue work towards an operational UMEPS. As part of the future development we will investigate the initial state perturbations with respect to spatial scale and error growth rate (e.g. Hohenegger and Schär, 2007) and sensitivity to spin-up time (e.g. Lean et al., 2008; Dixon et al., 2009). Since also too low model variability may lead to an underestimation of the uncertainty, a combination of different parameterization schemes among the UMEPS members may improve the ensemble forecast distributions as long as undesirable correlations between initial and physics perturbations are not introduced.

7. Acknowledgments

This research was partly funded by The Research Council of Norway trough the projects ArcChange, contract 178577/S30, and IPY-THORPEX, contract 175992/S30. The paper has made use of extra observations provided through the GTS during the campaign in March 2008, including data from the dropsondes released by the DLR Falcon research aircraft. Discussions and valuable contributions from Kevin Hodges, Marit H. Jensen, Gunnar Noer, Thor Erik Nordeng, Nigel Roberts and Øyvind Sætra are much appreciated. We appreciate the joint effort by Morten Salomonsen and Rune Bøe who provided radar observations of precipitation intensity. The authors also thank the two reviewers. In particular, the detailed suggestions made by Ken Mylne improved the paper.

References

Aakjær, P. D. 1992. Polar lows affecting Denmark. *Tellus* **44A**, 155–172.

Albright, M. D., Reed, R. J. and Ovens, D. W. 1995. Origin and structure of a numerically simulated polar low over Hudson Bay. *Tellus* **47A**, 834–848.

Anderson, D., Hodges, K. I. and Hoskins, B. J. 2003. Sensitivity of feature-based analysis methods of storm tracks to the form of background field removal. *Mon. Wea. Rev.* **131**, 565–573.

Aspelien, T., Bremnes, J. B., Frogner, I.-L. and Iversen, T. 2011. Short-range probabilistic forecasts from the Norwegian limited-area EPS. Long-term validation and a polar low study. *Tellus* **63A**, this issue.

Bechtold, P., Köhler, M., Jung, T., Doblas-Reyes, F., Leutbecher, M. and co-authors. 2008. Advances in simulating atmospheric variability with the ECMWF model: from synoptic to decadal time-scales. *Q. J. R. Meteor. Soc.* **134**, 1337–1351.

Blechschmidt, A.-M. 2008. A 2-year climatology of polar low events over the Nordic Seas from satellite remote sensing. *Geophys. Res. Lett.* **35**, L09815, doi:10.1029/2008GL033706.

Bowler, N. E. and Mylne, K. R. 2009. Ensemble transform Kalman filter perturbations for a regional ensemble prediction system. *Q. J. R. Meteor. Soc.* **135**, 757–766, doi:10.1002/qj.404.

Branković, Č., Matjačić, B., Ivatek-Šahdan, S. and Buizza, R. 2008. Downscaling of ECMWF ensemble forcasts for cases of severe weather: ensemble statistics and cluster analysis. *Mon. Wea. Rev.* **136**, 3323–3342.

Bratseth, A. M. 1985. A note on CISK in polar air masses. *Tellus* **37A**, 403–406.

Bracegirdle, T. J. and Gray, S. 2008. An objective climatology of the dynamical forcing of polar lows in the Nordic Seas. *Int. J. Climatol.* **28**, 1903–1919.

Buizza, R. 2002. Chaos and weather prediction. *European Centre for Medium-Range Weather, Internal Report; Meteorological Training Course*, 1–28.

Buizza, R. and Hollingsworth, A. 2002. Storm prediction over Europe using ECMWF Ensemble Prediction System. *Meteorol. Appl.* **9**, 289–305.

Buizza, R. and Palmer, T. N. 1995. The singular-vector structure of the atmospheric global circulation. *J. Atmos. Sci.* **52**, 1434–1456.

Buizza, R., Houtekamer, P. L., Pellerin, G., Toth, Z., Zhu, Y. and Wei, M. 2005. A comparison of the ECMWF, MSC, and NCEP global ensemble prediction systems. *Mon. Wea. Rev.* **133**, 1076–1097.

Buizza, R., Miller, M. and Palmer, T. N. 1999. Stochastic representation of model uncertainties in the ECMWF ensemble prediction system. *Q. J. R. Meteorol. Soc.* **125**, 2887–2908.

Businger, S. 1985. The synoptic climatology of polar low outbreaks. *Tellus* **37A**, 419–432.

Calvo, J. 2007. Kain-Fritsch convection in HIRLAM. Present status and prospects. *HIRLAM Newsletter* **52**, 57–64. Available at: http://hirlam.org/index.php?option=com_content&view=article&id=64&Itemid=101. Last accessed 28 Dec 2010.

Claud, C., Heinemann, G., Raustein, E. and McMurdie L. 2004. Polar low le Cygne: satellite observations and numerical simulations. *Q. J. R. Meteorol. Soc.* **130**, 1075–1102.

Cullen, M. J. P., Davies, T., Mawson, M. H., James, J. A., Coulter, S. C. and co-authors. 1997. An overview of numerical methods for the next generation UK NWP and climate model. In: *Numerical Methods in Atmospheric and Ocean Modelling: The Andre J. Robert Memorial Volume* (eds C. A. Lin, R. Laprise and H. Ritchie). Canadian Meteorological and Oceanographic Society, 425–444.

Davies, T., Cullen, M. J. P., Malcolm, A. J., Mawson, M. H., Staniforth, A. and co-authors. 2005. A new dynamical core for the Met Office's global and regional modelling of the atmosphere. *Q. J. R. Meteorol. Soc.* **131**. 1759–1782.

Dixon, M., Li, Z., Lean, H., Roberts, N. and Ballard, S. 2009. Impact of data assimilation on forecasting convection over the United Kingdom using a high-resolution version of the Met Office Unified Model. *Mon. Wea. Rev.* **137**, 1562–1584.

Emanuel, K. A. and Rotunno, R. 1989. Polar lows as arctic hurricanes. *Tellus* **41A**, 1–17.

Frogner, I.-L. and Iversen, T. 2001. Targeted ensemble prediction for northern Europe and parts of the north Atlantic Ocean. *Tellus* **53A**, 35–55.

Frogner, I.-L. and Iversen, T. 2002. High-resolution limited area ensemble predictions based on low-resolution targeted singular vectors. *Q. J. R. Meteorol. Soc.* **128**, 1321–1341.

Frogner, I.-L., Haakenstad, H. and Iversen, T. 2006. Limited area ensemble predictions at the Norwegian Meteorological Institute. *Q. J. R. Meteorol. Soc.* **132**, 2785–2808.

Froude, L. S. R., Bengtsson, L. and Hodges, K. I. 2007a. The predictbility of extratropical storm tracks and the sensitivity of their prediction of the observing system. *Mon. Wea. Rev.* **135**, 315–333.

Froude, L. S. R., Bengtsson, L. and Hodges, K. I. 2007b. The prediction of extratropical storm tracks by the ECMWF and NCEP ensemble prediction systems. *Mon. Wea. Rev.* **135**, 2545–2567.

Gustafsson, N., Källén, E. and Thorsteinsson, S. 1998. Sensitivity of forecast errors to initial and lateral boundary conditions. *Tellus* **50A**, 167–185.

Harold, J. M., Bigg, G. R. and Turner, J. 1999. Mesocyclone Acticity over the North-East Atlantic. Part 1: Vortex distribution and variability. *Int. J. Clim.* **19**, 1187–1204.

Harold, T. W. and Browning, K. A. 1969. The polar low as a baroclinic disturbance. *Q. J. Roy. Meteor. Soc.* **95**, 710–723.

Hodges, K. I. 1994. A general method for tracking analysis and its application to meteorological data. *Mon. Wea. Rev.* **120**, 2573–2586.

Hodges, K. I. 1995. Feature tracking on the unit sphere. *Mon. Wea. Rev.* **123**, 3458–3465.

Hodges, K. I. 1999. Adaptive constraints for feature tracking. *Mon. Wea. Rev.* **127**, 1362–1373.

Hohenegger, C. and Schär, C. 2007. Atmospheric predictability at synoptic versus cloud-resolving scales. *Bull. Am. Soc.* **88, 11**, 1783–1793. doi:10.1175/BAMS-88-11-1783

Hoskins, B. J. and Hodges, K. I. 2002. New perspective on the Northern Hemisphere Winter Storm Tracks. *J. Atmos. Sci.* **59**, 1041–1061.

Hoskins, B. J. and Hodges, K. I. 2005. New perspective on the Southern Hemisphere Storm Tracks. *J. Atmos. Sci.* **18**, 4108–4129.

Hoskins B. J., McIntyre, M. E. and Robertson, A. W. 1985. On the use and significance of isentropic potential vorticity maps. *Q. J. Roy. Meteor. Soc.* **111**, 877–946.

Ivarsson, K. I. 2007. The Rasch Kristjansson large scale condensation. Present status and prospects. *HIRLAM Newsletter* **52**, 50–56. Available at: http://hirlam.org/index.php?option=com_content&view=article&id=64&Itemid=101. Last accessed 28 Dec 2010.

Jung, T. and Leutbecher, M. 2008. Scale-dependent verification of ensemble forecasts. *Q. J. R. Meteorol. Soc.* **134**, 973–984.

Jung, T., Klinker, E. and Uppala, S. 2005. Reanalysis and reforecast of three major European storms of the twentieth century using ECMWF forecasting system. Part II: Ensemble forecasts. *Meteorol. Appl.* **12**, 111–122.

Kain, J. S., 2004. The Kain-Fritsch convective parameterization. An Update. *J. Appl. Meteor*. **43**, 170–181.

Kolstad, E. W. 2006. A new climatology of favourable conditions for reverse-shear polar lows. *Tellus* **58A**, 344–354.

Lean, H. W., Clark, P. A., Dixon, M., Roberts, N. M., Fitch, A. and co-authors. 2008. Characteristics of high-resolution versions of the Met Office Unified Model for forecasting convection over the United Kingdom. *Mon. Wea. Rev.* **136**, 3408–3424.

Leduc, M. and Laprise, R. 2009. Regional climate model sensitivity to domain size. *Clim Dyn.* **32**, 833–854.

Linders, T. and Saetra, Ø. 2010. Can CAPE maintain polar lows? *J. Atmos. Sci.* **67**, 2559–2571. (Referred to as LS10 in the text.)

Lopez, P. 2008. Comparison of OPERA precipitation radar composites to CMORPH, SYNOP and ECMWF model data. *ECMWF Technical Memorandum* **569**. Available at: www.ecmwf.int/publications. Last accessed 28 Dec 2010.

Mass, C. F., Ovens, D., Westrick, K. and Colle, B. A. 2002. Does increasing horizontal resolution produce more skillful forecasts. *Bull. Am. Meteorol. Soc.* **83**, 407–430.

McCabe, A. and Brown, A. R. 2007. The role of surface heterogeneity in modeling the stable boundary layer. *Boundary-Layer Meteorol.* **122**, 517–534.

King, J. C., Connolley, W. M. and Derbyshire, S. H. 2001. Sensitivity of modeled Antarctic climate to surface and boundary-layer flux parameterizations. *Q. J. R. Meteorol. Soc.* **127**, 779–794.

Molteni, F., Buizza, R., Palmer, T. N. and Petroliagis, T. 1996. The ECMWF ensemble prediction system; methodology and validation. *Q. J. R. Meteorol. Soc.* **122**, 73–119.

Montgomery, M. T. and Farrell, B. F. 1992. Polar low dynamics. *J. Atmos. Sci.* **49**, 2484–2505.

Nielsen, N. W. 1997. An early-autumn polar low formation over the Norwegian Sea. *J. Geophys. Res.* **102**(D12), 13,955–13, 973.

Noer, G. and Ovhed, M. 2003. Forecasting of polar lows in the Norwegian and the Barents Sea. In: *Proceedings of the 9th meeting of EGS Polar Lows Working Group*, Cambridge, UK. Available at: www.uni-trier.de/index.php?id=28161#c60628. Last accessed 28 Dec 2010.

Nordeng, T. E. 1990. A model-based diagnostic study of the development and maintenance mechanism of two polar lows. *Tellus* **42A**, 92–108.

Nordeng, T. E. and Rasmussen, E. A. 1992. A most beautiful polar low: a case study of a polar low development in the Bear Island region. *Tellus* **44A**, 81–99.

Økland, H., 1977. On the intensification of small-scale cyclones formed in very cold air masses heated by the ocean. *Institute Report Series*, Vol. 26, Department of Geophysics, University of Oslo.

Orrell, D., Smith, L., Barkmeijer, J. and Palmer, T. N. 2001. Model error in weather forecasting. *Nonl. Process. Geophys*. **8**, 357–371.

Paillux, J., Andersson, E. and Ondras, M. (eds.) 2008. Proceedings of the fourth WMO workshop on the impact of various observing systems on Numerical Weather Prediction. WMO Report WMO/TD No. 1450. Available at: www.wmo.int/pages/prog/ www/OSY/Reports/NWP-4_Geneva2008_index.html. Last accessed 28 Dec 2010.

Polar Low Special Issue. 1985. *Tellus* **37A**, 393–477.

Rabbe, Å. 1975. Arctic instability lows. *Meteorologiske Annaler* **6**, 303–329.

Rasch, P. J. and Kristjansson, J. E. 1998. A comparison of the CCM3 model climate using diagnosed and predicted condensate parameterizations. *J. Climate* **11**, 1587–1614.

Rasmussen, E. A. 1979. The polar low as an extratropical CISK disturbance. *Q. J. R. Meteorol. Soc.* **105**, 531–549.

Rasmussen, E. A. 1983. A review of meso-scale disturbances in cold air masses. In: *Mesoscale meteorology – theories, observations and models* (eds D. K. Lilly and T. Gal-Chen) D. Reidel Publishing Co. Dordrecht, Holland, 247–283.

Rassmussen, E. A. and Turner, J. (eds.). 2003. *Polar Lows: Mesoscale Weather Systems in the Polar Regions*. Cambridge University Press, 612 pp.

Roberts, N. M. 2000. The relationship between water vapour imagery and thunderstorms. *Internal Report (JCMM) no. 110.* Available at: www.metoffice.gov.uk. Last accessed 28 Dec 2010.

Roberts, N. 2003. The impact of a change to the use of the convection scheme to high resolution simulations of convective events. Stage 2 report from the strom-scale numerical modelling project. *Met Office Technical Report no. 407.* Available at: www.metoffice.gov.uk. Last accessed 28 Dec 2010.

Roberts, N. 2007. Meteorological components in forecasts of extreme convective rainfall using 12-km and 1-km NWP models: a tale of two storms. *Met Office Technical Report no. 520.* Available at: www.metoffice.gov.uk. Last accessed 28 Dec 2010.

Roberts, N. M. and Lean, H. W. 2008. Scale-selective verification of rainfall accumulations from high-resolution forecasts of convective events. *Mon. Wea. Rev.* **136**, 78–97.

Shapiro, M. A., Fedor, L. S. and Hampel, T. 1987. Researching aircraft measurements of a polar low over the Norwegian Sea. *Tellus* **39A**, 272–306.

Sørland, S. L. 2009. High-resolution ensemble forecasts of a polar low by non-hydrostatic downscaling. *Master thesis in Geosciences, Meteorology and Oceanography*. Department of Geosciences, University of Oslo. Available at: http://www.duo.uio.no/sok/work.html?WORKID=95171. Last accessed 28 Dec 2010.

Tijm, S. 2004. Hirlam pseudo satellite images. *HIRLAM Newsletter* **46**, 59–64.

Undén, P., Rounto, L., Järvinen, H., Lynch, P., Calvo, J. and co-authors. 2002. HIRLAM-5 Scientific Documentation, HIRLAM-5 project, c/o Per Undén SMHI, S-60176 Norrköping, Sweden.

van der Grijn, G. 2002. Tropical cyclone forecasting at ECMWF: new products and validation. *ECMWF Technical Memorandum* **386**. Available at: www.ecmwf.int/publications. Last accessed 28 Dec 2010.

Wilhelmsen, K. 1985. Climatological study of gale-producing polar lows near Norway. *Tellus* **37A**, 451–459.

Xue, Y., Vasic, R., Janjic, Z., Mesinger, F. and Mitchell, K. E. 2007. Assessment of dynamic downscaling of the continental U.S. regional climate using the Eta/SSiB Regional Climate Model. *J. Clim.* **20**, 4172–4193.

Yanase, W. and Niino, H. 2005. Effects of baroclinicity on the cloud pattern and structure of polar lows: a high-resolution numerical experiment. *Geophys. Res. Lett.* **32**, L02806, doi:10.1029/2004GL020469.

Yanase, W. and Niino, H. 2007. Dependence of polar low development on baroclinicity and physical processes. An idealized high-resolution numerical experiment. *J. Atmos. Sci.* **64**, 3044–3067.

Zahn, M. and Storch, H. V. 2008. Tracking polar lows in CLM. *Meteorologische Zeitschrift*, **17**, 445–453.

Zsoter, E., Buizza, R. and Richardson, R. 2009. "Jumpiness" of the ECMWF and Met Office EPS control and ensemble-mean forecasts. *Mon. Wea. Rev.* **137**, 3823–3836.